The many evolutionary fates of a large segmental duplication in mouse

Andrew P Morgan[1], J Matthew Holt[2], Rachel C McMullan[1], Timothy A Bell[1], Amelia M-F Clayshulte[1], John P Didion[1], Liran Yadgary[1], David Thybert[3], Duncan T Odom[4,5], Paul Flicek[3,5], Leonard McMillan[2], Fernando Pardo-Manuel de Villena[1]

[1] Department of Genetics, Carolina Center for Genome Sciences and Lineberger Comprehensive Cancer Center, University of North Carolina, Chapel Hill, NC

[2] Department of Computer Science, University of North Carolina, Chapel Hill, NC

[3] European Molecular Biology Laboratory, European Bioinformatics Institute, Wellcome Genome Campus, Hinxton, Cambridge, CB10 1SD, United Kingdom

[4] University of Cambridge, Cancer Research UK Cambridge Institute, Robinson Way, Cambridge, CB2 0RE, United Kindgom

[5] Wellcome Trust Sanger Institute, Wellcome Genome Campus, Hinxton, Cambridge, CB10 1SA, United Kingdom

Corresponding author:

Fernando Pardo-Manuel de Villena

5049 Genetic Medicine Building

120 Mason Farm Road CB#7264

Chapel Hill, NC 27599-7264

ABSTRACT

Gene duplication and loss are major sources of genetic polymorphism in populations, and are important forces shaping the evolution of genome content and organization. We have reconstructed the origin and history of a 127 kbp segmental duplication, *R2d*, in the house mouse (*Mus musculus*). *De novo* assembly of both the ancestral (*R2d1*) and the derived (*R2d2*) copies reveals that they have been subject to non-allelic gene conversion events spanning tens of kilobases. *R2d2* is also a hotspot for structural variation: its diploid copy number ranges from 0 in the mouse reference genome to more than 80 in wild mice sampled from around the globe. Heterozygosity for low- and high-copy alleles of *R2d2* is associated in *cis* with meiotic drive, suppression of meiotic crossovers, and copy-number instability, with a mutation rate in excess of 1% per generation in laboratory populations. We identify an additional 57 loci, covering 0.8% of the mouse genome, that have characteristics similar to *R2d2*: segmental duplication, phylogenetic discordance and low recombination rate. Our results provide a striking example of allelic diversity generated by duplication and demonstrate the value of *de novo* assembly in a phylogenetic context for understanding the mutational processes affecting duplicate genes.

INTRODUCTION

Duplication is an important force shaping the evolution of plant and animal genomes: redundant sequence provides both a substrate for evolution and transient relief from selective pressure (Lynch 2000). Like any sequence variant, a duplication first arises in a single individual in a population. Such polymorphisms are commonly called copy-number variants (CNVs) while segregating in the population, and segmental duplications (SDs) once fixed (Chain *et al.* 2014). The distinction between CNVs and SDs is somewhat arbitrary: tracts of SDs are highly polymorphic in populations in species from *Drosophila* (Dopman and Hartl 2007) to mouse (She *et al.* 2008) to human (Bailey and Eichler 2006), indicating that duplicated regions are hotspots for ongoing copy-number variation (CNV). Mutation rates for CNVs -- both gains and losses -- in SD-rich regions may be orders of magnitude higher than in unique sequence (Egan *et al.* 2007). This inherent instability is associated with speciation: in both the primate (Bailey and Eichler 2006) and mouse lineages, bursts of segmental duplication have preceded dramatic species radiations. Likewise, blocks of conserved synteny in mammals frequently terminate at SDs (Bailey and Eichler 2006), suggesting that SDs mediate the chromosomal rearrangements through which karyotypes diverge and reproductive barriers arise. Characterization of this "churning" in SD-rich regions is key to understanding the evolution of genome structure and function.

Notwithstanding their evolutionary importance, SDs are difficult to analyze. Repeated sequences with period longer than the insert size in a sequencing library and high pairwise similarity are likely to be collapsed into a single sequence during genome assembly. Efficient and sensitive alignment of high-throughput sequencing reads to duplicated sequence requires specialized software (Treangen and Salzberg 2011). Genotyping of sites within SDs is difficult because variants between copies (that is, paralogous variants) are easily confounded with variants within copies between individuals (that is, allelic variants.) Inability to distinguish allelic from paralogous variation similarly hampers any analysis that requires a positional ordering of sites along the genome -- for instance, delineation of haplotype blocks.

Paralogy also complicates phylogenetic inference. Ancestral duplication followed by differential losses along separate lineages yields a local phylogeny that is discordant with the genome-wide phylogeny (Goodman *et al.* 1979). Within each duplicate copy, local phylogenies for adjacent intervals may also be discordant due to non-allelic gene conversion between copies (Nagylaki and Petes 1982) -- despite the fact that such loci have reduced rates of crossing-over (Liu *et al.* 2014). The extremely high rate of gene conversion between palindromic repeats in the male-specific regions of mouse and human Y-chromosomes provide a dramatic example of this phenomenon (Hallast *et al.* 2013). As a result, over some fraction of the genome, individuals from the same species may be more closely related to an outgroup species than they are to each other.

In this manuscript we present a detailed analysis of one such paralogous sequence, *R2d*, in the house mouse *Mus musculus*. *R2d* is a 127 kbp unit which contains the protein-coding gene *Cwc22*. Although the C57BL/6J reference strain and other classical laboratory strains have a single copy of the *R2d* sequence (in the *R2d1* locus), the wild-derived CAST/EiJ, ZALENDE/EiJ, and WSB/EiJ strains have an additional 1, 16 and 33 copies respectively in the *R2d2* locus. *R2d2* is the responder locus in a recently-described meiotic drive system on mouse chromosome 2 but is absent from the mouse reference genome (Waterston *et al.* 2002; Didion *et al.* 2015, 2016). We draw on a collection of species from the genus *Mus* sampled from around the globe to reconstruct the sequence of events giving rise to the locus' present structure (**Figure 1**). Using novel computational tools built around indexes of raw high-throughput sequencing reads, we explore patterns of sequence divergence across the locus and perform local *de novo* assembly of phased haplotypes.

Both phylogenetic analyses and estimation of mutation rate in laboratory mouse populations reveal that *R2d2* and its surrounding region on chromsome 2 are exceptionally unstable in copy number. Cycles of duplication, deletion, retrotransposition and non-allelic gene conversion and loss have led to complex phylogenetic patterns discordant with species-level relationships within *Mus*.

Finally, we identify 57 other loci, covering 0.8% of the mouse genome, which share the features of *R2d2*: elevated local sequence divergence; low recombination rate; and enrichment for segmental duplication. Previous studies of sequence variation in the mouse (Keane *et al.* 2011) have attributed this pattern to sorting of alleles segregating in the common ancestor of *M. musculus* and its sister species. We suggest instead that these loci have been subject to independent cycles of duplication and loss along *Mus* lineages. Marked enrichment for odorant, pheromone, and antigen-recognition receptors supports a role for balancing selection on the generation and maintenance of the extreme level of polymorphism observed at these loci.

RESULTS

R2d was duplicated in the common ancestor of *M. musculus* and *M. spretus*

In order to determine when the *R2d* CNV arose, we used quantitative PCR or depth of coverage in whole-genome sequencing to assay *R2d* copy number in a collection of samples spanning the phylogeny of the subgenus *Mus*. Samples were classified as having haploid copy number 1 (two chromosomes each with a single copy of *R2d*), 2 (at least one chromosome with an *R2d* duplication) or >2 (both chromosomes with an *R2d* duplication).

We find evidence for >1 haploid copy in representatives of all mouse taxa tested from the Palearctic clade (Suzuki *et al.* 2004) (**Figure 1** and **Supplementary Table 1**): 202 of 496 *Mus musculus*, 1 of 1 *M. macedonicus*, 2 of 2 *M. spicilegus*, 1 of 1 *M. cypriacus* and 8 of 8 *M. spretus* samples. However, we find no evidence of duplication in species from the southeast Asian clade, which is an outgroup to Palearctic mice: 0 of 2 *M. famulus*, 0 of 2 *M. fragilicauda*, 0 of 1 *M. cervicolor*, 0 of 1 *M. cookii* and 0 of 1 *M. caroli* samples. Outside the subgenus *Mus*, we found evidence for >1 haploid copy in none of the 9 samples tested from subgenus *Pyromys*. We conclude that the *R2d* duplication most likely occurred between the divergence of southeast Asian from Palearctic mice (~3.5 million years ago [Mya]) and the divergence of *M. musculus* from *M. spretus* (~2 Mya) (Suzuki *et al.* 2004; Chevret *et al.* 2005), along the highlighted branch of the phylogeny in **Figure 1A**. If the *R2d* duplication is ancestral with respect to *M. musculus*, then extant lineages of laboratory mice which have a single haploid copy of *R2d* -- including the reference strain C57BL/6J (of predominantly *M. musculus domesticus* origin (Yang *et al.* 2007)) -- represent subsequent losses of an *R2d* paralog.

Duplication of the ancestral *R2d* sequence resulted in two paralogs residing in loci which we denote *R2d1* and *R2d2* (**Figure 1B**). Only one of these is present in the mouse reference genome, at chr2: 77.87 Mbp; the other copy maps approximately 6 Mbp distal (Didion *et al.* 2015), as we describe in more detail below. The more proximal copy, *R2d1*, lies in a region of conserved synteny with rat, rabbit, chimpanzee and human (Muffato *et al.* 2010) (**Supplementary Figure 1**); we conclude that it is the ancestral copy.

The sequence of the *R2d2* paralog was assembled *de novo* from whole-genome sequence reads (Keane *et al.* 2011) from the strain WSB/EiJ (of pure *M. m. domesticus* origin (Yang *et al.* 2011)), which has haploid *R2d* copy number ~34 (Didion *et al.* 2015). Pairwise alignment of *R2d2* against *R2d1* is shown in **Supplementary Figure 2**. The paralogs differ by at least 8 transposable-element (TE) insertions: 7 LINE

elements specific to *R2d1* and 1 endogenous retroviral element (ERV) specific to *R2d2* (**Supplementary Table 2**). (Due to the inherent limitations of assembling repetitive elements from short reads, it is likely that we have underestimated the number of young TEs in *R2d2*.) The *R2d1*-specific LINEs are all < 2% diverged from the consensus for their respective families in the RepeatMasker database (http://www.repeatmasker.org/cgi-bin/WEBRepeatMasker), consistent with insertion within the last 2 My. The oldest *R2d2*-specific ERV is 0.7% diverged from its family consensus. TE insertions occurring since the ancestral *R2d* duplication are almost certainly independent, so these data are consistent with duplication <2 Mya. The *R2d* unit, minus paralog-specific TE insertions, is 127 kbp in size. *R2d* units in the *R2d2* locus are capped on both ends by (CTCC)n microsatellite sequences, and no read pairs spanning the breakpoint between *R2d2* and flanking sequence were identified.

In order to obtain a more precise estimate of the molecular age of the duplication event we assembled *de novo* a total of 16.9 kbp of intergenic and intronic sequence in 8 regions across the *R2d* unit from diverse samples and constructed phylogenetic trees. The trees cover 17 *R2d1* or *R2d2* haplotypes -- 13 from inbred strains and 4 from wild mice. The sequence of *Mus caroli* (haploid copy number 1) is used as an outgroup. A representative tree is shown in **Figure 1C**. The *M. musculus* sequences form two clades representing *R2d1*- and *R2d2*-like sequence, respectively. Using 5.0 ± 1.0 million years before present (Mya) as the estimated divergence date for *M. caroli* and *M. musculus* (Suzuki *et al.* 2004; Chevret *et al.* 2005), Bayesian phylogenetic analysis with BEAST (Drummond *et al.* 2012) yields 1.6 Mya (95% HPD 0.7 − 5.1 Mya) as the estimated age of the duplication event. This estimate is consistent with the conclusion in **Figure 1A**.

R2d contains the essential gene *Cwc22*

The *R2d* unit encompasses one protein-coding gene, *Cwc22*, which encodes an essential mRNA splicing factor (Yeh *et al.* 2010). The gene is conserved across eukaryotes and is present in a single copy in most non-rodent species represented in the TreeFam database (http://www.treefam.org/family/TF300510 (Li 2006)). Five groups of *Cwc22* paralogs are present in mouse genomes: the copies in *R2d1* ($Cwc22^{R2d1}$) and *R2d2* ($Cwc22^{R2d2}$) plus retrotransposed copies in one locus at chr2: 83.9 Mbp and at two loci on the X chromosome (**Figure 2A**).

The three retrogenes are located in regions with no sequence homology to each other, indicating that each represents an independent retrotransposition event. The copy on chr2 was subsequently expanded by further segmental duplication and now exists (in the reference genome) in 7 copies with >99.9% mutual similarity. The two retrotransposed copies on chrX are substantially diverged from the parent gene (< 90% sequence similarity), lack intact open reading frames (ORFs), have minimal evidence of expression among GenBank cDNAs, and are annotated as likely pseudogenes (Pei *et al.* 2012). We therefore restricted our analyses to the remaining three groups of *Cwc22* sequences, all on chr2.

The canonical transcript of $Cwc22^{R2d1}$ (ENSMUST00000065889) is encoded by 21 exons on the negative strand. The coding sequence begins in the third exon and ends in the terminal exon (**Figure 2B**). Six of the seven protein-coding $Cwc22^{R2d1}$ transcripts in Ensembl v83 use this terminal exon, while one transcript (ENSMUST0000011824) uses an alternative terminal exon. Alignment of the retrogene sequence (ENSMUST00000178960) to the reference genome demonstrates that the retrogene captures the last 19 exons of the canonical transcript -- that is, the 19 exons corresponding to the coding sequence of the parent gene.

Copy number at *R2d2* is highly polymorphic in *M. musculus*

We previously demonstrated that haploid copy number of *R2d* ranges from 1 in the reference strain C57BL/6J and classical inbred strains A/J, 129S1/SvImJ, NOD/ShiLtJ, NZO/HILtJ; to 2 in the wild-derived

strain CAST/EiJ; to 34 in the wild-derived strain WSB/EiJ. Using linkage mapping in two multiparental genetic reference populations, the Collaborative Cross (Collaborative Cross Consortium 2012) and Diversity Outbred (Svenson *et al.* 2012), we showed that, for the two strains with haploid copy number >1, one copy maps to *R2d1* while all extra copies map to the *R2d2* locus at chr2: 83 Mbp (Didion *et al.* 2015). *Cwc22* was recently reported to have copy number as high as 83 in wild *M. m. domesticus* (Pezer *et al.* 2015).

In order to understand the evolutionary dynamics of copy-number variation at *R2d2*, we investigated the relationship between copy number and phylogeny in the *R2d2* candidate region. In particular, we sought evidence for or against a single common origin for each of the derived copy-number states (zero copies or many copies) at *R2d2*. The extent of copy-number variation in *M. musculus*, as estimated on a continuous scale by qPCR, is shown in **Figure 3A**; samples are colored according to their copy-number classification (1, 2 or >2 haploid copies). (Note that the qPCR readout is proportional to copy number on the log scale.) We confirmed that *R2d2* maps to chr2: 83 Mbp by performing association mapping between SNP genotypes from the MegaMUGA array (Morgan *et al.* 2016) and the qPCR readout (**Figure 3B**).

A phylogenetic tree was constructed using SNPs in the region of maximum association (chr2: 82 - 85 Mbp) and is shown in **Figure 3C**. The topology of the tree reflects predicted relationships: samples cluster by subspecies and (more loosely) by geography. Samples with a single *R2d* copy are present in all three subspecies and in every major branch within *M. m. domesticus*, supporting the conclusion that the *R2d2* paralog has been lost independently in multiple lineages. Several instances of intersubspecific introgression are evident: *M. m. musculus* into TW:DAJ (predominantly *M. m. castaneus*) and C57BR/cdJ (*M. m. domesticus*), and *M. m. domesticus* into CAST/EiJ (*M. m. castaneus*).

With two exceptions (SPRET/EiJ and TW:MEI; see **Discussion**), high-copy haplotypes are restricted to *M. m. domesticus*. They are present in classical inbred strains (ALR/LtJ, ALS/LtJ, CHMU/LeJ, and NU/J); in the ICR:HsD and related CD-1 commercial outbred stocks; in two inbred lines derived from ICR:HsD stock, HR8 (Swallow *et al.* 1998) and M16i (Rocha *et al.* 2004); and in wild-derived strains DDO, RBA/DnJ, RBB/DnJ, RBF/DnJ, WSA/EiJ, WSB/EiJ and ZALENDE/EiJ. In the wild, high-copy haplotypes are found in populations from across Europe and in the eastern United States. Although a clade representing mice of western European origin (highlighted in **Figure 3C**) is enriched for high-copy haplotypes, the most recent common ancestor of all samples with high copy number is basal to all *M. m. domesticus* surveyed.

The most highly associated SNP marker (JAX00494952 at chr2: 83,673,784) has only a weak correlation ($r^2 = 0.137$) with (log) copy number. High-copy haplotypes are thus poorly tagged in this dataset, and their apparently wide phylogenetic distribution in **Figure 3C** may be artefactual. To investigate further we turned to a partially overlapping dataset from the higher-density Mouse Diversity Array (MDA; (Yang *et al.* 2011)) containing 24 samples with copy number >2 (of which 5 are classical laboratory strains, 7 wild-derived strains, and 7 European wild mice; **Supplementary Table 1**). In fact all 24 high-copy samples are identical across a single 21 kbp interval, chr2: 83,896,447 - 83,917,565 (GRCm38/mm10 coordinates) (**Figure 3D**).

These analyses support a single origin within *Mus* for alleles with >2 copies and multiple origins for alleles with 1 copy.

Cwc22 is intact in and expressed from all *R2d* paralogs, and fast-evolving in rodents

To identify the coding sequence of $Cwc22^{R2d2}$ we first aligned the annotated transcript sequences of $Cwc22^{R2d1}$ from Ensembl to our *R2d2* contig. All 21 exons present in *R2d1* are present in *R2d2*. Then we used RNA-seq data from adult brain and testis in inbred strains with one or more copies of *R2d2* to

identify several novel transcript isoforms specific to *R2d2* (**Figure 4A**). First, we find evidence for frequent retention of the 12th and 18th introns in *Cwc22*^{R2d2} transcripts. The latter event can be explained by an A>G mutation at the 5′ splice donor site of exon 17 in *Cwc22*^{R2d2}. No variants were identified in the splice donor or acceptor sites for the 12th intron, but mis-splicing of this intron may be related to the presence of an ERV insertion (**Figure 4A**). Both intron-retention events would create an early stop codon. Second, we find evidence for a novel 3′ exon that extends to the boundary of the *R2d* unit and is used exclusively by *Cwc22*^{R2d2} (**Figure 4A**).

We estimated the expression of the various isoforms of *Cwc22*^{R2d1}, *Cwc22*^{R2d2} and retro-*Cwc22* in adult brain (8 replicates on 3 inbred strains) and testis (a single replicate on 23 inbred strains) using RNA-seq and the kallisto package (Bray *et al.* 2015). Briefly, kallisto uses an expectation-maximization (EM) algorithm to accurately estimate the abundance of a set of transcripts by distributing the "weight" of each read across all isoforms with whose sequence it is compatible. *Cwc22* is clearly expressed from all three paralogs in both brain and testis (**Figure 4B**). However, both the total expression and the pattern of isoform usage differ by tissue and copy number.

Next, we created a multiple sequence alignment and phylogenetic tree of *Cwc22* cDNAs and predicted amino acid sequences from *Cwc22*^{R2d1}, *Cwc22*^{R2d2}, retro-*Cwc22*, and *Cwc22* orthologs in 19 other placental mammals, plus opossum, platypus and finally chicken as an outgroup (**Supplementary Figure 3**). Ignoring the effects of retained introns in *Cwc22*^{R2d2}, an open reading frame (ORF) is maintained in all three *Cwc22* loci in mouse, including the retrogene. Information content of each column along the alignment (**Supplementary Figure 4**) reveals that sequence is most conserved in two predicted conserved domains, MIF4G and MA3, required for *Cwc22*'s function in mRNA processing (Yeh *et al.* 2010).

Maintenance of an ORF in all *Cwc22* paralogs for >2 My is evidence of negative selection against disrupting mutations in the coding sequence, but long branches within the rodent clade in **Supplementary Figure 3** suggest that *Cwc22* may also be under relaxed purifying selection in rodents. The rate of evolution of *Cwc22* sequences in mouse is faster than in the rest of the tree ($\chi^2 = 4.33$, df = 1, $p = 0.037$ by likelihood ratio test).

Phylogenetic discordance in *R2d1* is due to non-allelic gene conversion

The topology of trees across *R2d* is generally consistent: a long branch separating the single *M. caroli* sequence from the *M. musculus* sequences, and two clades corresponding to *R2d1*- and *R2d2*-like sequences. However, we observed that the affinities of some *R2d* paralogs change along the sequence (**Figure 5A**), a signature of non-allelic (*i.e.* inter-locus) gene conversion. To investigate further, we inspected patterns of sequence variation in whole-genome sequencing data from 16 wild-caught mice, 5 wild-derived strains, and 5 classical inbred strains of mice with a single *R2d* copy (at *R2d1*). We identified tracts of *R2d2*-like sequence as clusters of derived variants shared with our *R2d2* contig, and confirmed that they are physically contiguous with neighboring *R2d1* sequence by finding read pairs spanning the junction between *R2d1*- and *R2d2*-like sequence.

This analysis revealed non-allelic gene conversion tracts on at least 9 chromosomes (**Figure 5B**). The conversion tracts range in size from approximately 1.2 kbp to 127 kbp (the full length of the *R2d* unit). We require the presence of *R2d1*- or *R2d2*-diagnostic alleles at two or more consecutive variants to declare a conversion event, and these variants occur at a rate of approximately 1 per 50 bp, so the smallest conversion tracts we could detect are on the order of 100 bp in size. Nonetheless, the conversion tracts we detected are orders of magnitude longer than the 15 to 750 bp reported in recent studies of allelic gene conversion at recombination hotspots in mouse meiosis (Cole *et al.* 2010, 2014).

Four conversion tracts partially overlap the *Cwc22* gene to create a sequence that is a mosaic of *R2d1*- and *R2d2*-like exons (**Figure 5B**). Recovery of *Cwc22* mRNA in an inbred strain with a mosaic sequence (PWK/PhJ, see section "*Cwc22* is intact and expressed" below) indicates that transcription remains intact. The presence of both *R2d1*- and *R2d2*-like sequence in extant *M. musculus* lineages with a single copy of *R2d* reinforces our conclusion that the duplication is indeed ancestral to the divergence of *M. musculus* and that the reduction to haploid copy number 1 is a derived state.

In addition to exchanges between *R2d1* and *R2d2*, we identified an instance of exchange between *R2d2* and the adjacent retrotransposed copy of *Cwc22* in a single *M. m. domesticus* individual from Iran (IR:AHZ_STND:015; **Supplementary Figure 6**). A 30 kbp fragment corresponding to the 3' half of $Cwc22^{R2d2}$ was transposed into the retro-*Cwc22* locus, apparently mediated by homology between the exons of $Cwc22^{R2d2}$ and retro-*Cwc22*.

The genomic region containing *R2d2* is structurally unstable but has low sequence diversity

The extent of copy-number polymorphism and the frequency of non-allelic gene conversion involving *R2d2* suggest that it is relatively unstable. Consistent with these observations, we find that the rate of *de novo* copy-number changes at *R2d2* is extremely high in laboratory populations (**Figure 6**). In 183 mice sampled from the Diversity Outbred (DO) population we identified and confirmed through segregation analysis 8 new alleles, each with distinct copy number and each occurring in an unrelated haplotype (**Supplementary Table 3**). The DO is an outbred stock derived from eight inbred founder strains and maintained by random mating with 175 breeding pairs; at each generation, one male and one female offspring are sampled from each mating and randomly paired with a non-sibling to produce the next generation (Svenson *et al.* 2012). Without complete pedigrees and genetic material from breeders a direct estimate of the mutation rate in the DO is not straightforward to obtain. However, since the population size is known, we can make an analogy to microsatellite loci (Moran 1975) and estimate the mutation rate via the variance in allele sizes: 3.2% (95% bootstrap CI 1.1% − 6.0%) per generation.

Structural instability in this region of chr2 extends outside the *R2d2* locus itself. Less than 200 kbp distal to *R2d2* is another segmental duplication (**Figure 7**) -- containing a retrotransposed copy of *Cwc22* -- which is present in 7 tandem copies in the reference genome. That region, plus a further 80 kbp immediately distal to it, is copy-number polymorphic in wild *M. m. domesticus* and wild *M. m. castaneus* (**Figure 7**). Instability of the region over longer timescale is demonstrated by the disruption, just distal to the aforementioned segmental duplication, of a syntenic block conserved across all other mammals (**Supplementary Figure 1**).

Despite the high mutation rate for structural variants involving *R2d2* and nearby sequences, sequence diversity at the nucleotide level is modestly reduced relative to diversity in *R2d1* and relative to the genome-wide average in *M. m. domesticus*. In an approximately 200 kbp region containing the *R2d2* insertion site at its proximal end, $\hat{\pi}$ (an estimator of average heterozygosity) in *M. m. domesticus* reduced from approximately 0.3% (comparable to previous reports in this subspecies, (Salcedo *et al.* 2007)) to nearly zero (**Figure 7**). Divergence between *M. musculus* and *M. caroli* is similar to its genome-wide average of ~ 2.5% over the region.

Estimation of diversity *within* a duplicated sequence such as *R2d* is complicated by the difficulty of distinguishing allelic from paralogous variation. To circumvent this problem we split our sample of 26 wild *M. m. domesticus* into two groups: those having *R2d1* sequences only, and those having both *R2d1* and *R2d2* sequences. Within each group we counted the number of segregating sites among all *R2d2* copies, using nearby fixed differences between *R2d1* and *R2d2* to phase sites to *R2d2* (see **Methods** for

details), and used Watterson's estimator to calculate nucleotide diversity per site. Among *R2d1* sequences, $\theta = 0.25\% \pm 0.07\%$ versus $\theta = 0.048\% \pm 0.02\%$ among *R2d2* sequences (**Figure 7**) and $\theta = 0.17\% \pm 0.05\%$ among *R2d2* sequences in *M. m. castaneus*.

Churning of segmental duplications affects 0.8% of the mouse genome

The superposition of segmental duplication, non-allelic gene conversion, and recurrent loss -- which we collectively term "churning" -- of *R2d* paralogs mimics incomplete lineage sorting at *R2d1*. That is, the time to most recent common ancestor of *R2d1* haplotypes within the single-copy *M. musculus* samples is ~2 Mya, much older than the separation of the three *M. musculus* subspecies (**Figure 5**). We hypothesized that churning affects other segmentally duplicated sequences, and sought evidence for it at other loci in the mouse genome. To do so we identified regions where the divergence between sequenced samples and the reference genome assembly substantially exceeds what is predicted by those samples' ancestry. Because churning is likely to involve sequence that, like *R2d2*, is absent from the reference genome assembly, we developed a simple method to estimate divergence from unaligned reads. Briefly, we estimated the proportion of short subsequences (k-mers, with $k = 31$) from windows along the reference assembly for which no evidence exists in the reads generated for a sample. This quantity can be rescaled to approximate the divergence between the reference sequence and the template sequence from which reads were generated (see **Methods**). Applied genome-wide to 31 kbp ($= 1000\times k$) windows, this method captures the distribution of sequence divergence between the reference assembly (chiefly *M. m. domesticus* in origin) in representative samples from the three subspecies of *M. musculus* and the outgroups *M. spretus* and *M. caroli* (**Figure 8**).

Divergent regions were identified by fitting a hidden Markov model (HMM) to the windowed divergence profiles for 7 wild or wild-derived samples with available whole-genome sequence (**Figure 8** and **Supplementary Table 4**). This analysis revealed a striking pattern: over most of the genome, the divergence estimates hover around the genome-wide expectation, but high-divergence windows are clustered in regions 100 kbp to 5 Mbp in size. Our method does not capture signal from structural variation (besides deletions, see **Methods**) or heterozygosity, and so probably underestimates the true level of sequence divergence. The union of these divergent regions across all 7 *M. musculus* samples analyzed covers 0.82% of the reference genome (mean 0.58% per sample). Divergent regions are enriched for segmental duplications: 39.0% of sequence in divergent regions is comprised of segmental duplications versus a median of 3.4% (central 99% interval $0.2\% - 16.7\%$) in random regions of equal size ($p < 0.001$). Yet divergent regions are more gene-dense than the genomic background: they contain 3.6×10^{-2} genes/kbp relative a median 1.6×10^{-2} genes/kbp (central 99% interval 1.1×10^{-2} -- 2.7×10^{-2} genes/kbp) genome-wide ($p = < 0.001$). Divergent regions are strongly enriched for genes related to odorant and pheromone sensing ($p = 1.3\times10^{-8}$) and adaptive immunity ($p = 3.1\times10^{-3}$).

As a prototypical example we focus on a divergent region at chr4: 110 - 115 Mbp (**Figure 8**). This region contains the 11 members of the *Skint* family of T-cell-borne antigen receptors. The first member to be described, *Skint1*, functions in negative selection in the thymus of T-cells destined for the epidermis (Boyden *et al.* 2008). Coding sequence from 23 inbred strains (including CAST/EiJ, WSB/EiJ, PWD/PhJ and SPRET/EiJ) was reported in Boyden *et al*. (2008). A phylogenetic tree constructed from those sequences, plus *M. caroli* and rat as outgroups, reveals the expected pattern of "deep coalescence" (**Figure 8**): the *M. m. domesticus* sequences are paraphyletic, and some (group A) are more similar to SPRET/EiJ (*M. spretus*) than to their subspecific congeners (group B). Although the level of sequence divergence in the *Skint1* coding sequence was attributed to ancestral polymorphism maintained by balancing selection in the original report, selection would not be expected to maintain diversity in both coding and non-coding sequence equally as we observe in **Figure 8**. The best explanation for the observed pattern of diversity at

Skint1 is therefore that groups A and B represent paralogs descended from an ancestral duplication followed by subsequent deletion of different paralogs along different lineages (**Figure 8**). This conclusion is supported by the structure of the *Skint* region in the mouse reference genome assembly, which reflects the superposition of many duplications and rearrangements (**Figure 8**).

DISCUSSION

In this manuscript we have reconstructed in detail the evolution of a multi-megabase segmental duplication (SD) in mouse, *R2d2*. Our findings demonstrate the challenges involved in accurately interpreting patterns of polymorphism and divergence within duplicated sequence.

SDs are among the most dynamic loci in mammalian genomes. They are foci for copy-number variation in populations, but the sequences of individual duplicates beyond those present in the reference genome are often poorly resolved. Obtaining the sequence of this "missing genome," as we have done for *R2d2*, is an important prerequisite to understanding the evolution of duplicated loci. Since each paralog follows a partially independent evolutionary trajectory, individuals in a population may vary both quantitatively (in the number of copies) and qualitatively (in which copies are retained). Cycles of duplication and loss may furthermore lead to the fixation of different paralogs along different lineages. This "churning" leaves a signature of polymorphism far in excess of the genome-wide background, due to coalescence between alleles originating from distinct paralogs. We identify 57 additional regions covering 0.82% of the mouse genome with this property (**Figure 8**). These regions have gene density similar to unique sequence and are strongly enriched for genes involved in odorant sensing, pheromone recognition and immunity that play important roles in social behavior and speciation (Hurst *et al.* 2001). Excess polymorphism at these loci has previously been attributed to some combination of incomplete lineage sorting and diversifying selection (White *et al.* 2009; Keane *et al.* 2011). Our results suggest that inferences regarding the strength of selection on highly polymorphic loci in regions of genomic churn should be treated with caution.

Accurate deconvolution of recent duplications remains a difficult task that requires painstaking manual effort. We exploited the specific properties of *R2d2* in the WSB/EiJ mouse strain -- many highly-similar copies of *R2d2* relative to the single divergent *R2d1* copy -- to extract and assemble the sequence of *R2d2* from short reads (**Supplementary Figure 8**). With the sequence of both the *R2d1* and *R2d2* paralogs in hand, we were able to recognize several remarkable features of *R2d2* that are discussed in detail below.

Long-tract gene conversion.

Previous studies of non-allelic gene conversion in mouse and human have focused either on relatively small (<5 kbp) intervals within species, or have applied phylogenetic methods to multiple paralogs from a single reference genome (Dumont and Eichler 2013). This study is the first, to our knowledge, with the power to resolve large (>5 kbp) non-allelic gene conversion events on an autosome in a population sample. We identify conversion tracts up to 127 kbp in length, orders of magnitude longer than tracts arising from allelic conversion events during meiosis. Gene conversion at this scale can rapidly and dramatically alter paralogous sequences, including -- as shown in **Figure 5** -- the sequences of essential protein-coding genes. This process has been implicated as a source of disease alleles in humans (Chen *et al.* 2007).

Importantly, we were able to identify non-allelic exchanges in *R2d1* as such only because we were aware of the existence of *R2d2* in other lineages. In this case the transfer of paralogous *R2d2* sequence into *R2d1* creates the appearance of deep coalescence among *R2d1* sequences. Ignoring the effect of gene conversion

would cause us to overestimate the degree of polymorphism at *R2d1* by an order of magnitude, and would bias any related estimates of population-genetic parameters (for instance, of effective population size).

Our data are not sufficient to estimate the rate of non-allelic gene conversion between *R2d2* and other loci. At minimum we have observed two distinct events: one from *R2d2* into *R2d1*, and a second from *R2d2* into retro-*Cwc22*. From a single conversion event replacing all of *R2d1* with *R2d2*-like sequence, the remaining shorter conversion tracts could be generated by recombination with *R2d1* sequences. Because we find converted haplotypes in both *M. m. musculus* and *M. m. domesticus*, the single conversion event would have had to occur prior to the divergence of the three *M. musculus* subspecies and subsequently remain polymorphic in the diverged populations.

The other possibility is that non-allelic gene conversion between *R2d* sequences is recurrent. If this is the case, it probably also has a role in maintaining sequence identity between paralogs in *R2d2* -- an example of so-called "concerted evolution" (Dover 1982). Provided the rate of gene conversion is high enough relative to the rate of mutation, gene conversion in multi-copy sequences like *R2d2* tends to slow the accumulation of new mutations (Nagylaki and Petes 1982). New mutations arising in any single copy are prone to loss not only by drift but also by being "pasted-over" by gene conversion from other intact copies. The strength of this effect increases with copy number (Melamed and Kupiec 1992).

In this respect, *R2d2* appears similar to the male-specific region of the Y chromosome in mouse (Soh *et al.* 2014) and human (Rozen *et al.* 2003). The large palindromic repeats on chrY are homogenized by frequent non-allelic gene conversion (Hallast *et al.* 2013) such that they have retained >99% sequence identity to each other even after millions of years of evolution. Frequent non-allelic gene conversion has also been documented in arrays of U2 snRNA genes in human (Liao 1997), and in rRNA gene clusters (Eickbush and Eickbush 2007) and centromeric sequences (Schindelhauer 2002; Shi *et al.* 2010) in several species.

Pervasive copy-number variation.

Clusters of segmental duplications have long been known to be hotspots of copy-number variation (Bailey and Eichler 2006; Egan *et al.* 2007; She *et al.* 2008). Recent large-scale sequencing efforts have revealed the existence of thousands of multiallelic CNVs segregating in human populations (Handsaker *et al.* 2015), including cases of "runaway duplication" restricted to specific haplotypes. *R2d2* is another example of this phenomenon.

We have surveyed *R2d2* copy number in a large and diverse sample of laboratory and wild mice, and have shown that it varies from 0-1 (the ancestral state) to >80 in certain *M. m. domesticus* populations (**Figure 7**). In a cohort of outbred mice expected to be heterozygous for the WSB/EiJ haplotype at *R2d2* (33 copies) we estimate that large deletions, >2 Mbp in size, occur at a rate of 3.2% per generation. This estimate of the mutation rate for CNVs at *R2d2* should be regarded as a lower bound. The power of our copy-number assay to discriminate between copy numbers above ~25 is essentially zero, so that the assay is much more sensitive to losses than to gains. Even our lower-bound mutation rate exceeds that of the most common recurrent deletions in human (~1 per 7000 live births) (Turner *et al.* 2007) and is an order of magnitude higher than the most active CNV hotspots described to date in the mouse (Egan *et al.* 2007). While recurrent copy-number changes are often ascribed to non-allelic homologous recombination, the recombination rate in the vicinity of *R2d2* is dramatically reduced in populations segregating for *R2d2* haplotypes with high copy number (**Supplementary Figure 7**).

A second key observation is that both the recombination rate and the structural mutation rate at *R2d2* depend on heterozygosity. In contrast to estimates of mutation rate based on the number of alleles in

outbred populations (1% − 10% per generation), the copy number of *R2d2* appears to be stable over at least dozens of generations within inbred strains of mice, including in the Collaborative Cross (Collaborative Cross Consortium 2012). Mutation rate further differs by sex: zero new mutations were observed in 1256 progeny of females heterozygous for a high-copy allele at *R2d2* (data not shown).

Taken together, these observations hint at a common structural or epigenetic mechanism affecting the resolution of double-strand breaks in large tracts of unpaired (*i.e.* hemizygous) DNA during male meiosis. Both the obligate-hemizygous sex chromosomes and large unpaired segments on autosomes are epigenetically marked for transcriptional silencing during male meiotic prophase (Laan 2004; Baarends *et al.* 2005), and are physically sequestered into a structure called the sex body. Repair of double-strand breaks within the sex body is delayed relative to the autosomes (Mahadevaiah *et al.* 2001) and involves a different suite of proteins (Turner *et al.* 2004). We hypothesize that these male-specific pathway(s) are error-prone in the presence of non-allelic homologous sequences.

Origin and distribution of a meiotic driver.

Females heterozygous for a high- and low-copy allele at *R2d2* preferentially transmit the high-copy allele to progeny, a process called meiotic drive (Didion *et al.* 2015). Meiotic drive can rapidly alter allele frequencies in laboratory and natural populations (Lindholm *et al.* 2016), and we recently showed that high-copy alleles of *R2d2* (*R2d2*^{HC}) sweep through laboratory and natural populations despite reducing the fitness of heterozygous females (Didion *et al.* 2016). These "selfish sweeps" account for the marked reduction in within-population diversity in the vicinity of *R2d2* (**Figure 7**).

The present study sheds additional light on the age, origins and fate of *R2d2*^{HC} alleles. We find that *R2d2*^{HC} alleles have a single origin in western Europe. They are present in several different "chromosomal races" -- populations fixed for specific Robertsonian translocations between which gene flow is limited (Hauffe and Searle 1993) -- indicating that they were likely present at intermediate frequency prior to the origin of the chromosomal races within the past 6,000 to 10,000 years (Nachman *et al.* 1994) and were dispersed through Europe as mice colonized the continent from the south and east (Boursot *et al.* 1993). The presence of *R2d2*^{HC} in non-*M. m. domesticus* samples (SPRET/EiJ, *M. spretus* from Cadiz, Spain; and TW:MEI, *M. m. castaneus* from Taiwan) is best explained by recent introgression following secondary contact with *M. m. domesticus* (Bonhomme *et al.* 2007; Yang *et al.* 2011).

A new member of the *Cwc22* family.

The duplication that gave rise to *R2d2* also created a new copy of *Cwc22*. Based on our assembly of the *R2d2* sequence, the open reading frame of *Cwc22*^{R2d2} is intact and encodes a nearly full-length predicted protein that retains the two key functional domains characteristic of the *Cwc22* family. Inspection of RNA-seq data from samples with high copy number at *R2d2* reveals several novel transcript isoforms whose expression appears to be copy-number- and tissue-dependent. In testis, the most abundant isoform retains an intron containing an ERV insertion (red arrow in **Figure 4**), consistent with the well-known transcriptional promiscuity in this tissue. The most abundant isoforms in adult brain is unusual in that its stop codon is in an internal exon which is followed by a 7 kbp 3′ UTR in the terminal exon. Transcripts with a stop codon in an internal exon are generally subject to nonsense-mediated decay (NMD) triggered by the presence of exon-junction complexes downstream the stop codon. Curiously, *Cwc22* is itself a member of the exon-junction complex (Steckelberg *et al.* 2012).

That an essential gene involved in such a central biochemical pathway should both escape NMD and be overexpressed more than tenfold is surprising. However, it may be the case that standing levels of *Cwc22*^{R2d2} transcript do not reflect levels of the functional *Cwc22* protein. Either of the two intron-retention

events in **Figure 4** would introduce early stop codons and consequently be subject to NMD or produce a truncated and likely nonfunctional protein. Further studies will be required to determine the distribution of expression of *Cwc22* across isoforms, tissues and developmental stages.

Conclusions and future directions

Our detailed analysis of the evolutionary trajectory of *R2d2* provides insight into the fate of duplicated sequences over short (within-species) timescales. The exceptionally high mutation rate and low recombination rate at *R2d2* motivate hypotheses regarding the biochemical mechanisms which contribute to observed patterns of polymorphism at this and similar loci. Finally, the birth of a new member of the deeply conserved *Cwc22* gene family in *R2d2* provides an opportunity to test predictions regarding the evolution of duplicate gene pairs.

METHODS

Mice

Wild *M. musculus* mice used in this study were trapped at a large number of sites across Europe, the United States, the Middle East, northern India and Taiwan (**Figure 7A**). Trapping was carried out in accordance with local regulations and with the approval of all relevant regulatory bodies for each locality and institution. Trapping locations are listed in **Supplementary Table 1**. Most samples have been previously published (Didion *et al.* 2016).

Tissue samples from the progenitors of the wild-derived inbred strains ZALENDE/EiJ (*M. m. domesticus*), TIRANO/EiJ (*M. m. domesticus*) and SPRET/EiJ (*M. spretus*) were provided by Muriel Davisson, as described in Didion *et al.* (2016).

Tissue samples from the high running (HR) selection and intercross lines were obtained as described in Didion *et al.* (2016).

Female Diversity Outbred mice used for estimating mutation rates at *R2d2* were obtained from the Jackson Laboratory and housed with a single FVB/NJ male. Progeny were sacrificed at birth by cervical dislocation in order to obtain tissue for genotyping.

All live laboratory mice were handled in accordance with the IACUC protocols of the University of North Carolina at Chapel Hill.

DNA preparation

High molecular weight DNA. High molecular weight DNA was obtained for samples genotyped with the Mouse Diversity Array or subject to whole-genome sequencing. Genomic DNA was extracted from tail, liver or spleen using a standard phenol-chloroform procedure (Sambrook and Russell 2006). High molecular weight DNA for most inbred strains was obtained from the Jackson Laboratory, and the remainder as a generous gift from Francois Bonhomme and the University of Montpellier Wild Mouse Genetic Repository.

Low molecular weight DNA. Low molecular weight DNA was obtained for samples to be genotyped on the MegaMUGA array (see "Microarray genotyping" below). Genomic DNA was isolated from tail, liver, muscle or spleen using Qiagen Gentra Puregene or DNeasy Blood & Tissue kits according to the manufacturer's instructions.

Whole-genome sequencing and variant discovery

Inbred strains. Sequencing data for inbred strains of mice except ZALENDE/EiJ and LEWES/EiJ was obtained from the Sanger Mouse Genomes Project website (ftp://ftp-mouse.sanger.ac.uk/current_bams) as aligned BAM files. Details of the sequencing pipeline are given in Keane *et al.* (2011). Coverage ranged from approximately 25X to 50X per sample.

The strains LEWES/EiJ and ZALENDE/EiJ were sequenced at the University of North Carolina High-Throughput Sequencing Facility. Libraries were prepared from high molecular weight DNA using the Illumina TruSeq kit and insert size approximately 250 bp, and 2x100bp paired-end reads were generated on an Illumina HiSeq 2000 instrument. LEWES/EiJ was sequenced to approximately 12X coverage and ZALENDE/EiJ to approximately 20X. Alignment was performed as in Keane *et al.* (2011).

Wild mice. Whole-genome sequencing data from 26 wild *M. m. domesticus* individuals described in Pezer *et al.* (2015) was downloaded from ENA under accession #PRJEB9450. Coverage ranged from approximately 12X to 20X per sample. An additional two wild *M. m. domesticus* individuals, IT175 and ES446, were sequenced at the University of North Carolina to approximate coverage 8X each. Raw reads from an additional 10 wild *M. m. castaneus* described in Halligan *et al.* (2013), sequenced to approximately 20X each, were downloaded from ENA under accession #PRJEB2176. Reads for a single *Mus caroli* individual sequenced to approximately 40X were obtained from ENA under accession #PRJEB2188. Reads for each sample were realigned to the mm10 reference using bwa-mem v0.7.12 with default parameters (Li 2013). Optical duplicates were removed with samblaster (Faust and Hall 2014).

Variant discovery. Polymorphic sites on chromosome 2 in the vicinity of *R2d2* (**Figure 7**) were called using freebayes v0.9.21-19-gc003c1e (Garrison and Marth 2012) with parameters "--standard-filters" using the Sanger Mouse Genomes Project VCF files as a list of known sites (parameter "--@"). Raw calls were filtered to have quality score > 30, root mean square mapping quality > 20 (for both reference and alternate allele calls) and at most 2 alternate alleles.

Copy-number estimation

R2d copy number was estimated using qPCR as described in Didion *et al.* (2016). Briefly, we used commercial TaqMan assays against intron-exon boundaries in *Cwc22* (Life Technologies assay numbers Mm00644079_cn and Mm00053048_cn) to determine copy number relative to reference genes *Tert* (cat. no. 4458368, for target Mm00644079_cn) or *Tfrc* (cat. no. 4458366, for target Mm00053048_cn). Cycle thresholds for *Cwc22* relative to the reference gene were normalized across assay batches using linear mixed models with batch and target-reference pair treated as random effects. Control samples with known haploid *R2d* copy numbers of 1 (C57BL/6J), 2 (CAST/EiJ), 17 (WSB/EiJxC57BL/6J)F_1 and 34 (WSB/EiJ) were included in each batch.

Samples were classified as having 1, 2 or >2 haploid copies of *R2d* using linear discriminant analysis. The classifier was trained on the normalized cycle thresholds of the control samples from each plate, whose precise integer copy number is known, and applied to the remaining samples.

Microarray genotyping

Genome-wide genotyping was performed using MegaMUGA, the second version of the Mouse Universal Genotyping Array platform (Neogen/GeneSeek, Lincoln, NE) (Morgan *et al.* 2016). Genotypes were called using the GenCall algorithm implemented in the Illumina BeadStudio software (Illumina Inc, Carlsbad, CA). For quality control we computed, for each marker i on the array: $S_i = X_i + Y_i$, where X_i and Y_i are

the normalized hybridization intensities for the two alleles. The expected distribution of Si was computed from a large set of reference samples. We excluded arrays for which the distribution of S_i was substantially shifted from this reference; in practice, failed arrays can be trivially identified in this manner (Morgan *et al.* 2016). Access to MegaMUGA genotypes was provided by partnership between the McMillan and Pardo-Manuel de Villena labs and the UNC Systems Genetics Core Facility.

Additional genotypes for inbred strains and wild mice from the Mouse Diversity Array were obtained from Yang *et al.* (2011).

De novo assembly of *R2d2*

Raw whole-genome sequencing reads for WSB/EiJ from the Sanger Mouse Genomes Project were converted to a multi-string Burrows-Wheeler transform and associated FM-index (msBWT) (Holt and McMillan 2014) using the msbwt v0.1.4 Python package (https://pypi.python.org/pypi/msbwt). The msBWT and FM-index implicitly represent a suffix array of sequencing to provide efficient queries over arbitrarily large string sets. Given a seed k-mer present in that string set, this property can be exploited to rapidly construct a de Bruijn graph which can in turn be used for local *de novo* assembly of a target sequence (**Supplementary Figure 8A**). The edges in that graph can be assigned a weight (corresponding to the number of reads containing the $k + 1$-mer implied by the edge) which can be used to evaluate candidate paths when the graph branches (**Supplementary Figure 8B**).

R2d2 was seeded with the 30 bp sequence (TCTAGAGCATGAGCCTCATTTATCATGCCT) at the proximal boundary of *R2d1* in the GRCm38/mm10 reference genome. A single linear contig was assembled by "walking" through the local de Bruijn graph. Because WSB/EiJ has ~33 copies of *R2d2* and a single copy of *R2d1*, any branch point in the graph which represents a paralogous variant should having outgoing edges with weights differing by a factor of approximately 33. Furthermore, when two (or more) branch points occur within less than the length of a read, it should be possible to "phase" the underlying variants by following single reads through both branch points (**Supplementary Figure 8B**). We used these heuristics to assemble the sequence of *R2d2* (corresponding to the higher-weight path through the graph) specifically.

After assembling a chunk of approximately 500 bp the contig was checked for colinearity with the reference sequence (*R2d1*) using BLAT and CLUSTAL-W2 (using the EMBL-EBI web server: http://www.ebi.ac.uk/Tools/msa/clustalw2/).

Repetitive elements such as retroviruses are refractory to assembly with our method. Upon traversing into a repetitive element, the total edge weight (total number of reads) and number of branch points (representing possible linear assembled sequences) in the graph become large. It was sometimes possible to assemble a fragment of a repetitive element at its junction with unique sequence but not to assemble unambiguously across the repeat. Regions of unassembleable sequence were marked with blocks of Ns, and assembly re-seeded using a nearby *k*-mer from the reference sequence. The final contig is provided in FASTA format in **Supplementary File 1**.

The final contig was checked against its source msBWT by confirming that each 30-mer in the contig which did not contain an N was supported by at least 60 reads. A total of 16 additional haplotypes in 8 regions of *R2d* totaling 16.9 kbp (**Supplementary Table 5**) were assembled in a similar fashion, using the WSB *R2d2* contig and the *R2d1* reference sequence as guides. Multiple sequence alignments from these regions are provided in **Supplementary File 1**.

Sequence analysis of *R2d2* contig

Pairwise alignment of R2d *paralogs.* The reference *R2d1* sequence and our *R2d2* contig were aligned using LASTZ v1.03.54 (http://www.bx.psu.edu/~rsharris/lastz/) with parameters "--step=10 --seed=match12 --notransition --exact=20 --notrim --identity=95".

Transposable element (TE) content. The *R2d2* contig was screened for TE insertions using the RepeatMasker web server (http://www.repeatmasker.org/cgi-bin/WEBRepeatMasker) with species set to "mouse" and default settings otherwise. As noted previously, we could not assemble full-length repeats, but the fragments we could assemble at junctions with unique sequence allowed identification of some candidate TEs to the family level. *R2d1*-specific TEs were defined as TEs annotated in the RepeatMasker track at the UCSC Genome Browser with no evidence (no homologous sequence, and no Ns) at the corresponding position in the *R2d2* contig. Candidate *R2d2*-specific TEs were defined as gaps >= 100 bp in size in the alignment to *R2d1* for which the corresponding *R2d2* sequence was flagged by RepeatMasker.

Gene conversion tracts. Using multiple sequence alignments (see "Phylogenetic analyses" below) of the 8 *de novo* assembled regions in *R2d*, we classified each sequence as *R2d1*-like or *R2d2*-like based on the pattern of shared derived alleles (using *M. caroli* as the outgroup). The result of this analysis is shown in **Supplementary Figure 5**.

To unambiguously define gene conversion events in a larger sample, and without confounding from paralogous sequence, we examined 12 wild *M. m. domesticus* samples and 8 laboratory strains with evidence of 2 diploid copies of *R2d*. We first confirmed that these copies of *R2d* were located at *R2d1* by finding read pairs spanning the junction between *R2d1* and neighboring sequence. Gene conversion tracts were delineated by manual inspection of alignments in IGV. Because *R2d1* and *R2d2* diverged approximately 2 Mya, alignment of *R2d2*-like sequence to the *R2d1* reference sequence creates mismatches at a density of approximately 1 variant per 50 bp, approximately fivefold greater than the density of variants in wild *M. m. domesticus* (~ 0.4% or 1 per 250 bp; (Salcedo *et al.* 2007)). Boundaries of conversion tracts were defined at approximately the midpoint between the first *R2d1*- (or *R2d2*-) specific variant and the last *R2d2*- (or *R2d1*-) specific variant.

Sequence diversity in R2d1 *and* R2d2. Assembling individual copies of *R2d2* is infeasible in high-copy samples. Instead we treated each *R2d* unit as an independent sequence and used the number of segregating sites to estimate sequence diversity. Segregating sites were defined as positions in a collection of alignments (BAM files) with evidence of an alternate allele. To identify segregating sites we used freebayes v0.9.21-19-gc003c1e (Garrison and Marth 2012) with parameters "-ui -Kp 20 --use-best-n-alleles 2 -m 8". These parameters treat each sample as having ploidy up to 20, impose an uninformative prior on genotype frequencies, and limit the algorithm to the discovery of atomic variants (SNVs or short indels, not multinucleotide polymorphisms or other complex events) with at most 2 alleles at each segregating site. Sites in low-complexity sequence (defined as Shannon entropy < 1.6 in the 30 bp window centered on the site) or within 10 bp of another variant site were further masked, to minimize spurious calls due to ambiguous alignment of indels. To avoid confounding with the retrocopies of *Cwc22* outside *R2d*, coding exons of *Cwc22* were masked. Finally, sites corresponding to an unaligned or gap position in the pairwise alignment between *R2d1* and *R2d2* were masked.

To compute diversity in *R2d1* we counted segregating sites in 12 wild *M. m. domesticus* samples with 2 diploid copies of *R2d* (total of 24 sequences), confirmed to be in *R2d1* by the presence of read pairs spanning the junction between *R2d1* and neighboring sequence. To compute diversity in *R2d2*, we counted segregating sites in 14 wild *M. m. domesticus* samples with >2 diploid copies of *R2d* (range 3 -- 83 per sample; total of 406 sequences) but excluded sites corresponding to variants among *R2d1* sequences.

Remaining sites were phased to *R2d2* by checking for the presence of a 31-mer containing the site and the nearest *R2d1*-vs-*R2d2* difference in the raw reads for each sample using the corresponding msBWT. Sequence diversity was then computed using Watterson's estimator (Watterson 1975), dividing by the number of alignable bases (128973) to yield a per-site estimate. Standard errors were estimated by 100 rounds of resampling over the columns in the *R2d1*-vs-*R2d2* alignment.

Analyses of *Cwc22* expression

RNA-seq read alignment. Expression of *Cwc22* was examined in adult whole brain using data from Crowley *et al.* (2015), SRA accession #SRP056236. Paired-end reads (2x100bp) were obtained from 8 replicates each of 3 inbred strains: CAST/EiJ, PWK/PhJ and WSB/EiJ. Raw reads were aligned to the mm10 reference using STAR v2.4.2a (Dobin *et al.* 2012) with default parameters for paired-end reads. Alignments were merged into a single file per strain for further analysis. Expression in adult testis was examined in 23 wild-derived inbred strains from Phifer-Rixey *et al.* (2014) SRA accession #PRJNA252743. Single-end reads (76bp) were aligned to the mm10 genome with STAR using default parameters for single-end, non-strand-specific reads.

Transcript assembly. Read alignments were manually inspected to assess support for *Cwc22* isoforms in Ensembl v83 annotation. To identify novel isoforms in *R2d2*, we applied the Trinity v0.2.6 pipeline (Grabherr *et al.* 2011) to the subset of reads from WSB/EiJ which could be aligned to *R2d1* plus their mates (a set which represents a mixture of $Cwc22^{R2d1}$ and $Cwc22^{R2d2}$ reads). De novo transcripts were aligned both to the mm10 reference and to the *R2d2* contig using BLAT, and were assigned to *R2d1* or *R2d2* based on sequence similarity. Because expression from *R2d2* is high in WSB/EiJ, *R2d2*-derived transcripts dominated the assembled set. Both manual inspection and the Trinity assembly indicated the presence of retained introns and an extra 3′ exon, as described in the **Results**. To obtain a full set of Cwc22 transcripts including those of both *R2d1* and *R2d2* origin, we supplemented the *Cwc22* transcripts in Ensembl v83 with their paralogs from *R2d2* as determined by a strict BLAT search against the *R2d2* contig. We manually created additional transcripts reflecting intron-retention and 3′ extension events described above, and obtained their sequence from the *R2d2* contig.

Abundance estimation. Relative abundance of *Cwc22* paralogs was estimated using kallisto v0.42.3 (Bray *et al.* 2015) with parameters "--bias" (to estimate and correct library-specific sequence-composition biases). The transcript index used for pseudoalignment and quantification included only the *Cwc22* targets.

Phylogenetic analyses

Trees. Multiple sequence alignments for 8 the regions in **Supplementary Figure 5** were generated using MUSCLE (Edgar 2004) with default parameters. The resulting alignments were manually trimmed and consecutive gaps removed. Phylogenetic trees were inferred with RAxML v8.1.9 (Stamatakis 2014) using the GTR+gamma model with 4 rate categories and *M. caroli* as an outgroup. Uncertainty of tree topologies was evaluated using 100 bootstraps replicates.

Divergence time. The time of the split between *R2d1* and *R2d2* was estimated using the Bayesian method implemented in BEAST v1.8.1r6542 (Drummond *et al.* 2012). We assumed a divergence time for *M. caroli* of 5 Mya and a strict molecular clock, and analyzed the alignment from region A in **Supplementary Figure 5** under the GTR+gamma model with 4 rate categories and allowance for a proportion of invariant sites. The chain was run for 10 million iterations with trees sampled every 1000 iterations.

Local phylogeny around R2d2. Genotypes from the MegaMUGA array at 38 SNPs in the region surrounding *R2d2* (chr2: 82 -- 85 Mb) were obtained for 493 individuals representing both laboratory and wild mice

(**Supplementary Table 1**). A distance matrix was created by computing the proportion of alleles shared identical by state between each pair of samples. A neighbor-joining tree was inferred from the distance matrix and rooted at the most recent common ancestor of the *M. musculus*- and non-*M. musculus* samples. **Figure 3** shows a simplified tree with 135 representative samples, including all those with high-copy alleles at *R2d2*.

Cwc22 *coding sequences*. To create the tree of Cwc22 coding sequences, we first obtained the sequences of all its paralogs in mouse. The coding sequence of *Cwc22*^{R2d1} (RefSeq transcript NM_030560.5) was obtained from the UCSC Genome Browser and aligned to our *R2d2* contig with BLAT to extract the exons of *Cwc22*^{R2d2}. The coding sequence of retro-*Cwc22* (genomic sequence corresponding to GenBank cDNA AK145290) was obtained from the UCSC Genome Browser. Coding and protein sequences of *Cwc22* homologs from non-*M. musculus* species were obtained from Ensembl (Cunningham *et al.* 2014). The sequences were aligned with MUSCLE and manually trimmed, and a phylogenetic tree estimated as described above.

We observed that the branches in the rodent clade of the *Cwc22* tree appeared to be longer than branches for other taxa. We used PAML (Yang *et al.* 2007) to test the hypothesis that *Cwc22* is under relaxed purifying selection in rodents using the branch-site model (null model "model = 2, NSsites = 2, fix_omega = 1"; alternative model "model = 2, NSsites = 2, omega = 1, fix_omega = 1") as described in the PAML manual. This is a test of difference in evolutionary rate on a "foreground" branch (ω_1) -- in our case, the rodent clade -- relative to the tree-wide "background" rate (ω_0). The distribution of the test statistic is an even mixture of a χ^2 distribution with 1 df and a point mass at zero; to obtain the p-value, we calculated the quantile of the χ^2 distribution with 1 df and divided by 2.

Genome-wide sequence divergence

The msBWT of a collection of whole-genome sequencing reads can be used to estimate the divergence between the corresponding template sequence (*i.e.* genome) and a reference sequence as follows. Non-overlapping k-mers from the reference sequence are queried against the msBWT. (The value of k is chosen such that nearly all k-mers drawn from genomic sequence exclusive of repetitive elements.) Let x be the count of reads containing an exact match to the k-mer or its reverse complement. If the template and reference sequence are identical, standard theory for shotgun sequencing (Lander and Waterman 1988) holds that $P(x > 0|\lambda) = 1 - e^{-\lambda}$, where λ is the average sequencing coverage. We assume $P(x > 0|\lambda) \approx 1$, which is satisfied in practice for high-coverage sequencing.

However, if a haploid template sequence contains at least one variant (versus the reference) within the queried k-mer, it will be the case that $x = 0$. We use this fact and assume that mutations arise along a sequence via a Poisson process to estimate the rate parameter α from the proportion of k-mers that have read count zero. Let m be the number of mutations arising between a target and reference in a window of length L, and y the number of k-mers in that window with nonzero read count. Then $P(m = 0|\alpha) = e^{-\alpha L}$ and a simple estimator for α is $\hat{\alpha} = -\log\left(\frac{1-y}{L}\right)$.

Interpretation of α is straightforward in the haploid case: it is the per-base rate of sequence divergence between the template sequence and the reference sequence. In the diploid case it represents a lower bound on the sequence divergence of the two homologous chromosomes.

We applied this estimator with $k = 31$ and $L = 1000 \times k = 31$ kbp to msBWTs for 7 inbred strains (3 *M. m. domesticus*, 1 *M. m. musculus*, 1 *M. m. castaneus*, 1 *M. spretus*, 1 *M. caroli*) and 2 wild *M. m. domesticus* individuals (IT175, ES446) using the GRCm38/mm10 mouse reference sequence as the source of k-mer

queries. As shown in **Figure 8**, the mode of the distribution of divergence values matches what is expected based on the ancestry of the samples with respect to the reference. To identify divergent regions, we fit a discrete-time hidden Markov model (HMM) to the windows divergence values. The HMM had two hidden states: "normal" sequence, with emission distribution $N(0.005,0.005)$ and initial probability 0.99; and "divergent" sequence, with emission distribution $N(0.02,0.005)$ and initial probability 0.01. The transmission probability between states was 1×10^{-5}. Posterior decodings were obtained via the Viterbi algorithm, as implemented in the R package HiddenMarkov (https://cran.r-project.org/package=HiddenMarkov).

Significance tests for overlap with genomic features were performed using the resampling algorithm implemented in the Genomic Association Tester (GAT) package for Python (https://pypi.python.org/pypi/gat). Segmental duplications were obtained from the genomicSuperDups table of the UCSC Genome Browser and genes from Ensembl v83 annotation.

Analyses of recombination rate at *R2d2*

To test the effect of *R2d2* copy number on local recombination rate we estimated the difference between observed and expected (based on the most recent mouse genetic map (Liu *et al.* 2014)) recombination fraction in 11 experimental crosses in which one of the parental lines was segregating for a high-copy allele at *R2d2*. Genotype data was obtained from The Jackson Laboratory's Mouse Phenome Database QTL Archive (http://phenome.jax.org/db/q?rtn=qtl/home). Recombination fractions were calculated using R/qtl (http://rqtl.org/). Confidence intervals for difference between observed and expected recombination fractions were calculated by 100 iterations of nonparametric bootstrapping over individuals in each dataset.

We also examined recombination events accumulated during the first 18 generations of breeding of the Diversity Outbred (DO) population, in which the high-copy *R2d2* allele from WSB/EiJ is segregating. Founder haplotype reconstructions were obtained for each of the DO individuals reported in (Didion *et al.* 2016), and recombination events were identified as junctions between founder haplotypes. We compared the frequency of junctions involving a WSB/EiJ haplotype to junctions not involving a WSB/EiJ haplotype over the region chr2: 75-90 Mb.

Results of these analyses are presented in **Supplementary Figure 7**.

Data availability

All *de novo* assemblies used in this study are included in **Supplementary File 1**. The data structures on which the assemblies are based, and the interactive computational tools used for assembly, are publicly available at http://www.csbio.unc.edu/CEGSseq/index.py?run=MsbwtTools.

Acknowledgments

We thank all the scientists and personnel who collected and processed the wild mouse samples used in this study. In particular we thank Francois Bonhomme for providing samples from wild-derived inbred strains housed at the University of Montpellier Wild Mouse Genetic Repository, and Ted Garland for providing tissue samples from the HR selection lines and related crosses. This work was supported by National Institutes of Health grants P50GM076468 (FPMdV), U19AI100625 (FPMdV, APM), F30MH103925 (APM), T32GM067553 (JPD, APM), and by Vaadia-BARD Postdoctoral Fellowship Award

FI-12 478-13 to LY. Additional support was provided by Cancer Research UK, the European Research Council, EMBO Young Investigator Programme (DTO), European Molecular Biology Laboratory (DTO, PF) and the Wellcome Trust (WT095908) (PF) and (WT098051) (PF, DTO); and finally by the European Union's Seventh Framework Programme (FP7/2007-2013) under grant agreement HEALTH-F4-2010-241504 (EURATRANS).

REFERENCES

Baarends W. M., Wassenaar E., Laan R. van der, Hoogerbrugge J., Sleddens-Linkels E., Hoeijmakers J. H. J., Boer P. de, Grootegoed J. A., 2005 Silencing of unpaired chromatin and histone H2A ubiquitination in mammalian meiosis. Mol Cell Biol **25**: 1041–1053.

Bailey J. A., Eichler E. E., 2006 Primate segmental duplications: Crucibles of evolution, diversity and disease. Nat Rev Genet **7**: 552–564.

Bonhomme F., Rivals E., Orth A., Grant G. R., Jeffreys A. J., Bois P. R., 2007 Species-wide distribution of highly polymorphic minisatellite markers suggests past and present genetic exchanges among house mouse subspecies. Genome Biol **8**: R80.

Boursot P., Auffray J. C., Britton-Davidian J., Bonhomme F., 1993 The evolution of house mice. Annu Rev Ecol Syst **24**: 119–152.

Boyden L. M., Lewis J. M., Barbee S. D., Bas A., Girardi M., Hayday A. C., Tigelaar R. E., Lifton R. P., 2008 Skint1, the prototype of a newly identified immunoglobulin superfamily gene cluster, positively selects epidermal T cells. Nat Genet **40**: 656–662.

Bray N., Pimentel H., Melsted P., Patcher L., 2015 Near-optimal RNA-seq quantification. arXiv.

Chain F. J. J., Feulner P. G. D., Panchal M., Eizaguirre C., Samonte I. E., Kalbe M., Lenz T. L., Stoll M., Bornberg-Bauer E., Milinski M., Reusch T. B. H., 2014 Extensive copy-number variation of young genes across stickleback populations. PLoS Genet **10**: e1004830.

Chen J.-M., Cooper D. N., Chuzhanova N., Férec C., Patrinos G. P., 2007 Gene conversion: Mechanisms, evolution and human disease. Nat Rev Genet **8**: 762–775.

Chevret P., Veyrunes F., Britton-Davidian J., 2005 Molecular phylogeny of the genus Mus (Rodentia: Murinae) based on mitochondrial and nuclear data. Biol J Linn Soc **84**: 417–427.

Cole F., Keeney S., Jasin M., 2010 Comprehensive, fine-scale dissection of homologous recombination outcomes at a hot spot in mouse meiosis. Mol Cell **39**: 700–710.

Cole F., Baudat F., Grey C., Keeney S., Massy B. de, Jasin M., 2014 Mouse tetrad analysis provides insights into recombination mechanisms and hotspot evolutionary dynamics. Nat Genet **46**: 1072–1080.

Collaborative Cross Consortium, 2012 The genome architecture of the Collaborative Cross mouse menetic reference population. Genetics **190**: 389–401.

Crowley J. J., Zhabotynsky V., Sun W., Huang S., Pakatci I. K., Kim Y., Wang J. R., Morgan A. P., Calaway J. D., Aylor D. L., Yun Z., Bell T. A., Buus R. J., Calaway M. E., Didion J. P., Gooch T. J., Hansen S. D., Robinson N. N., Shaw G. D., Spence J. S., Quackenbush C. R., Barrick C. J., Nonneman R. J., Kim K.,

788 Xenakis J., Xie Y., Valdar W., Lenarcic A. B., Wang W., Welsh C. E., Fu C.-P., Zhang Z., Holt J., Guo Z.,
789 Threadgill D. W., Tarantino L. M., Miller D. R., Zou F., McMillan L., Sullivan P. F., Villena F. P.-M. de,
790 2015 Analyses of allele-specific gene expression in highly divergent mouse crosses identifies pervasive
791 allelic imbalance. Nat Genet **47**: 353–360.

792 Cunningham F., Amode M. R., Barrell D., Beal K., Billis K., Brent S., Carvalho-Silva D., Clapham P.,
793 Coates G., Fitzgerald S., Gil L., Giron C. G., Gordon L., Hourlier T., Hunt S. E., Janacek S. H., Johnson N.,
794 Juettemann T., Kahari A. K., Keenan S., Martin F. J., Maurel T., McLaren W., Murphy D. N., Nag R.,
795 Overduin B., Parker A., Patricio M., Perry E., Pignatelli M., Riat H. S., Sheppard D., Taylor K., Thormann
796 A., Vullo A., Wilder S. P., Zadissa A., Aken B. L., Birney E., Harrow J., Kinsella R., Muffato M., Ruffier M.,
797 Searle S. M. J., Spudich G., Trevanion S. J., Yates A., Zerbino D. R., Flicek P., 2014 Ensembl 2015. Nucleic
798 Acids Res **43**: D662–D669.

799 Dallas J. F., 1992 Estimation of microsatellite mutation rates in recombinant inbred strains of mouse.
800 Mamm Genome **3**: 452–456.

801 Didion J. P., Morgan A. P., Clayshulte A. M.-F., Mcmullan R. C., Yadgary L., Petkov P. M., Bell T. A., Gatti
802 D. M., Crowley J. J., Hua K., Aylor D. L., Bai L., Calaway M., Chesler E. J., French J. E., Geiger T. R.,
803 Gooch T. J., Garland T., Harrill A. H., Hunter K., McMillan L., Holt M., Miller D. R., O'Brien D. A., Paigen
804 K., Pan W., Rowe L. B., Shaw G. D., Simecek P., Sullivan P. F., Svenson K. L., Weinstock G. M., Threadgill
805 D. W., Pomp D., Churchill G. A., Villena F. P.-M. de, 2015 A multi-megabase copy number gain causes
806 maternal transmission ratio distortion on mouse chromosome 2. PLoS Genet **11**: e1004850.

807 Didion J. P., Morgan A. P., Yadgary L., Bell T. A., McMullan R. C., Solorzano L. O. de, Britton-Davidian J.,
808 Bult C. J., Campbell K. J., Castiglia R., Ching Y.-H., Chunco A. J., Crowley J. J., Chesler E. J., Förster D. W.,
809 French J. E., Gabriel S. I., Gatti D. M., Garland T., Giagia-Athanasopoulou E. B., Giménez M. D., Grize S.
810 A., Gündüz I., Holmes A., Hauffe H. C., Herman J. S., Holt J. M., Hua K., Jolley W. J., Lindholm A. K.,
811 López-Fuster M. J., Mitsainas G., Luz Mathias M. da, McMillan L., Ramalhinho M. G., Rehermann B.,
812 Rosshart S. P., Searle J. B., Shiao M.-S., Solano E., Svenson K. L., Thomas-Laemont P., Threadgill D. W.,
813 Ventura J., Weinstock G. M., Pomp D., Churchill G. A., Villena F. P.-M. de, 2016 R2d2 drives selfish
814 sweeps in the house mouse. Mol Biol Evol: msw036.

815 Dobin A., Davis C. A., Schlesinger F., Drenkow J., Zaleski C., Jha S., Batut P., Chaisson M., Gingeras T. R.,
816 2012 STAR: Ultrafast universal RNA-seq aligner. Bioinformatics **29**: 15–21.

817 Dopman E. B., Hartl D. L., 2007 A portrait of copy-number polymorphism in drosophila melanogaster.
818 Proceedings of the National Academy of Sciences **104**: 19920–19925.

819 Dover G., 1982 Molecular drive: A cohesive mode of species evolution. Nature **299**: 111–117.

820 Drummond A. J., Suchard M. A., Xie D., Rambaut A., 2012 Bayesian phylogenetics with BEAUti and the
821 BEAST 1.7. Mol Biol Evol **29**: 1969–1973.

822 Dumont B. L., Eichler E. E., 2013 Signals of historical interlocus gene conversion in human segmental
823 duplications. PLoS ONE **8**: e75949.

824 Edgar R. C., 2004 MUSCLE: Multiple sequence alignment with high accuracy and high throughput.
825 Nucleic Acids Res **32**: 1792–1797.

826 Egan C. M., Sridhar S., Wigler M., Hall I. M., 2007 Recurrent DNA copy number variation in the
827 laboratory mouse. Nat Genet **39**: 1384–1389.

828 Eickbush T. H., Eickbush D. G., 2007 Finely orchestrated movements: Evolution of the ribosomal RNA
829 genes. Genetics **175**: 477–485.

830 Faust G. G., Hall I. M., 2014 SAMBLASTER: Fast duplicate marking and structural variant read
831 extraction. Bioinformatics **30**: 2503–2505.

832 Garrison E., Marth G., 2012 Haplotype-based variant detection from short-read sequencing. arXiv.

833 Goodman M., Czelusniak J., Moore G. W., Romero-Herrera A. E., Matsuda G., 1979 Fitting the gene
834 lineage into its species lineage, a parsimony strategy illustrated by cladograms constructed from globin
835 sequences. Syst Biol **28**: 132–163.

836 Grabherr M. G., Haas B. J., Yassour M., Levin J. Z., Thompson D. A., Amit I., Adiconis X., Fan L.,
837 Raychowdhury R., Zeng Q., Chen Z., Mauceli E., Hacohen N., Gnirke A., Rhind N., Palma F. di, Birren B.
838 W., Nusbaum C., Lindblad-Toh K., Friedman N., Regev A., 2011 Full-length transcriptome assembly from
839 RNA-seq data without a reference genome. Nat Biotechnol **29**: 644–652.

840 Hallast P., Balaresque P., Bowden G. R., Ballereau S., Jobling M. A., 2013 Recombination dynamics of a
841 human Y-chromosomal palindrome: Rapid GC-biased gene conversion, multi-kilobase conversion tracts,
842 and rare inversions. PLoS Genet **9**: e1003666.

843 Halligan D. L., Kousathanas A., Ness R. W., Harr B., Eöry L., Keane T. M., Adams D. J., Keightley P. D.,
844 2013 Contributions of protein-coding and regulatory change to adaptive molecular evolution in murid
845 rodents. PLoS Genet **9**: e1003995.

846 Handsaker R. E., Doren V. V., Berman J. R., Genovese G., Kashin S., Boettger L. M., McCarroll S. A., 2015
847 Large multiallelic copy number variations in humans. Nat Genet **47**: 296–303.

848 Hauffe H. C., Searle J. B., 1993 Extreme karyotypic variation in a Mus musculus domesticus hybrid zone:
849 The tobacco mouse story revisited. Evolution **47**: 1374.

850 Holt J., McMillan L., 2014 Merging of multi-string BWTs with applications. Bioinformatics **30**: 3524–3531.

851 Hurst J. L., Payne C. E., Nevison C. M., Marie A. D., Humphries R. E., Robertson D. H. L., Cavaggioni A.,
852 Beynon R. J., 2001 Individual recognition in mice mediated by major urinary proteins. Nature **414**: 631–
853 634.

854 Keane T. M., Goodstadt L., Danecek P., White M. A., Wong K., Yalcin B., Heger A., Agam A., Slater G.,
855 Goodson M., Furlotte N. A., Eskin E., Nellåker C., Whitley H., Cleak J., Janowitz D., Hernandez-Pliego P.,
856 Edwards A., Belgard T. G., Oliver P. L., McIntyre R. E., Bhomra A., Nicod J., Gan X., Yuan W., Weyden L.
857 van der, Steward C. A., Bala S., Stalker J., Mott R., Durbin R., Jackson I. J., Czechanski A., Guerra-
858 Assunção J. A., Donahue L. R., Reinholdt L. G., Payseur B. A., Ponting C. P., Birney E., Flint J., Adams D.
859 J., 2011 Mouse genomic variation and its effect on phenotypes and gene regulation. Nature **477**: 289–294.

860 Laan R. van der, 2004 Ubiquitin ligase Rad18Sc localizes to the XY body and to other chromosomal
861 regions that are unpaired and transcriptionally silenced during male meiotic prophase. J Cell Sci **117**:
862 5023–5033.

863 Lander E. S., Waterman M. S., 1988 Genomic mapping by fingerprinting random clones: A mathematical
864 analysis. Genomics **2**: 231–239.

865 Li H., 2006 TreeFam: A curated database of phylogenetic trees of animal gene families. Nucleic Acids Res
866 **34**: D572–D580.

867 Li H., 2013 Aligning sequence reads, clone sequences and assembly contigs with BWA-MEM. arXiv.

868 Liao D., 1997 Concerted evolution of the tandemly repeated genes encoding human U2 snRNA (the
869 RUN2 locus) involves rapid intrachromosomal homogenization and rare interchromosomal gene
870 conversion. EMBO J **16**: 588–598.

871 Lindholm A. K., Dyer K. A., Firman R. C., Fishman L., Forstmeier W., Holman L., Johannesson H., Knief
872 U., Kokko H., Larracuente A. M., Manser A., Montchamp-Moreau C., Petrosyan V. G., Pomiankowski A.,
873 Presgraves D. C., Safronova L. D., Sutter A., Unckless R. L., Verspoor R. L., Wedell N., Wilkinson G. S.,
874 Price T. A., 2016 The ecology and evolutionary dynamics of meiotic drive. Trends Ecol Evol.

875 Liu E. Y., Morgan A. P., Chesler E. J., Wang W., Churchill G. A., Villena F. P.-M. de, 2014 High-resolution
876 sex-specific linkage maps of the mouse reveal polarized distribution of crossovers in male germline.
877 Genetics **197**: 91–106.

878 Lynch M., 2000 The evolutionary fate and consequences of duplicate genes. Science **290**: 1151–1155.

879 Mahadevaiah S. K., Turner J. M., Baudat F., Rogakou E. P., Boer P. de, Blanco-Rodríguez J., Jasin M.,
880 Keeney S., Bonner W. M., Burgoyne P. S., 2001 Nat Genet **27**: 271–276.

881 Melamed C., Kupiec M., 1992 Effect of donor copy number on the rate of gene conversion in the yeast
882 Saccharomyces cerevisiae. Mol Genet Genom **235**: 97–103.

883 Moran P., 1975 Wandering distributions and the electrophoretic profile. Theor Popul Biol **8**: 318–330.

884 Morgan A. P., Fu C.-P., Kao C.-Y., Welsh C. E., Didion J. P., Yadgary L., Hyacinth L., Ferris M. T., Bell T.
885 A., Miller D. R., Giusti-Rodriguez P., Nonneman R. J., Cook K. D., Whitmire J. K., Gralinski L. E., Keller
886 M., Attie A. D., Churchill G. A., Petkov P., Sullivan P. F., Brennan J. R., McMillan L., Villena F. P.-M. de,
887 2016 The Mouse Universal Genotyping Array: From substrains to subspecies. G3 **6**.

888 Muffato M., Louis A., Poisnel C. E., Crollius H. R., 2010 Genomicus: A database and a browser to study
889 gene synteny in modern and ancestral genomes. Bioinformatics **26**: 1119–1121.

890 Nachman M. W., Boyer S. N., Searle J. B., Aquadro C. F., 1994 Mitochondrial DNA variation and the
891 evolution of robertsonian chromosomal races of house mice, Mus domesticus. Genetics **136**: 1105–1120.

892 Nagylaki T., Petes T. D., 1982 Intrachromosomal gene conversion and the maintenance of sequence
893 homogeneity among repeated genes. Genetics **100**: 315–337.

894 Pei B., Sisu C., Frankish A., Howald C., Habegger L., Mu X., Harte R., Balasubramanian S., Tanzer A.,
895 Diekhans M., Reymond A., Hubbard T. J., Harrow J., Gerstein M. B., 2012 The GENCODE pseudogene
896 resource. Genome Biol **13**: R51.

Pezer, Harr B., Teschke M., Babiker H., Tautz D., 2015 Divergence patterns of genic copy number variation in natural populations of the house mouse (Mus musculus domesticus) reveal three conserved genes with major population-specific expansions. Genome Res **25**: 1114–1124.

Phifer-Rixey M., Bomhoff M., Nachman M. W., 2014 Genome-wide patterns of differentiation among house mouse subspecies. Genetics **198**: 283–297.

Rocha J. L., Eisen E. J., Vleck L. D. V., Pomp D., 2004 A large-sample QTL study in mice: I. Growth. Mamm Genome **15**: 83–99.

Rozen S., Skaletsky H., Marszalek J. D., Minx P. J., Cordum H. S., Waterston R. H., Wilson R. K., Page D. C., 2003 Abundant gene conversion between arms of palindromes in human and ape Y chromosomes. Nature **423**: 873–876.

Salcedo T., Geraldes A., Nachman M. W., 2007 Nucleotide variation in wild and inbred mice. Genetics **177**: 2277–2291.

Sambrook J., Russell D. W. (Eds.), 2006 *Molecular cloning: A laboratory manual*. Cold Spring Harbor Laboratory Press.

Schindelhauer D., 2002 Evidence for a fast, intrachromosomal conversion mechanism from mapping of nucleotide variants within a homogeneous alpha-satellite DNA array. Genome Res **12**: 1815–1826.

She X., Cheng Z., Zöllner S., Church D. M., Eichler E. E., 2008 Mouse segmental duplication and copy number variation. Nat Genet **40**: 909–914.

Shi J., Wolf S. E., Burke J. M., Presting G. G., Ross-Ibarra J., Dawe R. K., 2010 Widespread gene conversion in centromere cores. PLoS Biol **8**: e1000327.

Soh Y., Alföldi J., Pyntikova T., Brown L., Graves T., Minx P., Fulton R., Kremitzki C., Koutseva N., Mueller J., Rozen S., Hughes J., Owens E., Womack J., Murphy W., Cao Q., de~Jong P., Warren W., Wilson R., Skaletsky H., Page D., 2014 Sequencing the mouse Y chromosome reveals convergent gene acquisition and amplification on both sex chromosomes. Cell **159**: 800–813.

Stamatakis A., 2014 RAxML version 8: A tool for phylogenetic analysis and post-analysis of large phylogenies. Bioinformatics **30**: 1312–1313.

Steckelberg A.-L., Boehm V., Gromadzka A., Gehring N., 2012 Cwc22 connects pre-mRNA splicing and exon junction complex assembly. Cell Rep **2**: 454–461.

Suzuki H., Shimada T., Terashima M., Tsuchiya K., Aplin K., 2004 Temporal, spatial, and ecological modes of evolution of Eurasian Mus based on mitochondrial and nuclear gene sequences. Mol Phylogenet Evol **33**: 626–646.

Svenson K. L., Gatti D. M., Valdar W., Welsh C. E., Cheng R., Chesler E. J., Palmer A. A., McMillan L., Churchill G. A., 2012 High-resolution genetic mapping using the mouse Diversity Outbred population. Genetics **190**: 437–447.

Swallow J. G., Carter P. A., Jr. T. G., 1998 Artificial selection for increased wheel-running behavior in house mice. Behav Genet **28**: 227–237.

933 Treangen T. J., Salzberg S. L., 2011 Repetitive DNA and next-generation sequencing: Computational
934 challenges and solutions. Nat Rev Genet.

935 Turner J. M., Aprelikova O., Xu X., Wang R., Kim S., Chandramouli G. V., Barrett J., Burgoyne P. S., Deng
936 C.-X., 2004 BRCA1, histone H2AX phosphorylation, and male meiotic sex chromosome inactivation. Curr
937 Biol **14**: 2135–2142.

938 Turner D. J., Miretti M., Rajan D., Fiegler H., Carter N. P., Blayney M. L., Beck S., Hurles M. E., 2007
939 Germline rates of de novo meiotic deletions and duplications causing several genomic disorders. Nat
940 Genet **40**: 90–95.

941 Waterston R. H., Chinwalla A. T., Cook L. L., Delehaunty K. D., Fewell G. A., Fulton L. A., Fulton R. S.,
942 Graves T. A., Hillier L. W., Mardis E. R., McPherson J. D., Miner T. L., Nash W. E., Nelson J. O., Nhan M.
943 N., Pepin K. H., Pohl C. S., Ponce T. C., Schultz B., Thompson J., Trevaskis E., Waterston R. H., Wendl M.
944 C., Wilson R. K., Yang S.-P., An P., Berry E., Birren B., Bloom T., Brown D. G., Butler J., Daly M., David R.,
945 Deri J., Dodge S., Foley K., Gage D., Gnerre S., Holzer T., Jaffe D. B., Kamal M., Karlsson E. K., Kells C.,
946 Kirby A., Kulbokas E. J., Lander E. S., Landers T., Leger J. P., Levine R., Lindblad-Toh K., Mauceli E.,
947 Mayer J. H., McCarthy M., Meldrim J., Meldrim J., Mesirov J. P., Nicol R., Nusbaum C., Seaman S., Sharpe
948 T., Sheridan A., Singer J. B., Santos R., Spencer B., Stange-Thomann N., Vinson J. P., Wade C. M.,
949 Wierzbowski J., Wyman D., Zody M. C., Birney E., Goldman N., Kasprzyk A., Mongin E., Rust A. G.,
950 Slater G., Stabenau A., Ureta-Vidal A., Whelan S., Ainscough R., Attwood J., Bailey J., Barlow K., Beck S.,
951 Burton J., Clamp M., Clee C., Coulson A., Cuff J., Curwen V., Cutts T., Davies J., Eyras E., Grafham D.,
952 Gregory S., Hubbard T., Hunt A., Jones M., Joy A., Leonard S., Lloyd C., Matthews L., McLaren S., McLay
953 K., Meredith B., Mullikin J. C., Ning Z., Oliver K., Overton-Larty E., Plumb R., Potter S., Quail M., Rogers
954 J., Scott C., Searle S., Shownkeen R., Sims S., Wall M., West A. P., Willey D., Williams S., Abril J. F., Guigó
955 R., Parra G., Agarwal P., Agarwala R., Church D. M., Hlavina W., Maglott D. R., Sapojnikov V.,
956 Alexandersson M., Pachter L., Antonarakis S. E., Dermitzakis E. T., Reymond A., Ucla C., Baertsch R.,
957 Diekhans M., Furey T. S., Hinrichs A., Hsu F., Karolchik D., Kent W. J., Roskin K. M., Schwartz M. S.,
958 Sugnet C., Weber R. J., Bork P., Letunic I., Suyama M., Torrents D., Zdobnov E. M., Botcherby M., Brown
959 S. D., Campbell R. D., Jackson I., Bray N., Couronne O., Dubchak I., Poliakov A., Rubin E. M., Brent M. R.,
960 Flicek P., Keibler E., Korf I., Batalov S., Bult C., Frankel W. N., Carninci P., Hayashizaki Y., Kawai J.,
961 Okazaki Y., Cawley S., Kulp D., Wheeler R., Chiaromonte F., Collins F. S., Felsenfeld A., Guyer M.,
962 Peterson J., Wetterstrand K., Copley R. R., Mott R., Dewey C., Dickens N. J., Emes R. D., Goodstadt L.,
963 Ponting C. P., Winter E., Dunn D. M., Niederhausern A. C. von, Weiss R. B., Eddy S. R., Johnson L. S.,
964 Jones T. A., Elnitski L., Kolbe D. L., Eswara P., Miller W., O'Connor M. J., Schwartz S., Gibbs R. A.,
965 Muzny D. M., Glusman G., Smit A., Green E. D., Hardison R. C., Yang S., Haussler D., Hua A., Roe B. A.,
966 Kucherlapati R. S., Montgomery K. T., Li J., Li M., Lucas S., Ma B., McCombie W. R., Morgan M., Pevzner
967 P., Tesler G., Schultz J., Smith D. R., Tromp J., Worley K. C., Lander E. S., Abril J. F., Agarwal P.,
968 Alexandersson M., Antonarakis S. E., Baertsch R., Berry E., Birney E., Bork P., Bray N., Brent M. R., Brown
969 D. G., Butler J., Bult C., Chiaromonte F., Chinwalla A. T., Church D. M., Clamp M., Collins F. S., Copley R.
970 R., Couronne O., Cawley S., Cuff J., Curwen V., Cutts T., Daly M., Dermitzakis E. T., Dewey C., Dickens
971 N. J., Diekhans M., Dubchak I., Eddy S. R., Elnitski L., Emes R. D., Eswara P., Eyras E., Felsenfeld A.,
972 Flicek P., Frankel W. N., Fulton L. A., Furey T. S., Gnerre S., Glusman G., Goldman N., Goodstadt L.,
973 Green E. D., Gregory S., Guigó R., Hardison R. C., Haussler D., Hillier L. W., Hinrichs A., Hlavina W.,
974 Hsu F., Hubbard T., Jaffe D. B., Kamal M., Karolchik D., Karlsson E. K., Kasprzyk A., Keibler E., Kent W.
975 J., Kirby A., Kolbe D. L., Korf I., Kulbokas E. J., Kulp D., Lander E. S., Letunic I., Li M., Lindblad-Toh K.,
976 Ma B., Maglott D. R., Mauceli E., Mesirov J. P., Miller W., Mott R., Mullikin J. C., Ning Z., Pachter L.,
977 Parra G., Pevzner P., Poliakov A., Ponting C. P., Potter S., Reymond A., Roskin K. M., Sapojnikov V.,

978 Schultz J., Schwartz M. S., Schwartz S., Searle S., Singer J. B., Slater G., Smit A., Stabenau A., Sugnet C.,
979 Suyama M., Tesler G., Torrents D., Tromp J., Ucla C., Vinson J. P., Wade C. M., Weber R. J., Wheeler R.,
980 Winter E., Yang S.-P., Zdobnov E. M., Whelan S., Worley K. C., Zody M. C., 2002 Initial sequencing and
981 comparative analysis of the mouse genome. Nature **420**: 520–562.

982 Watterson G., 1975 On the number of segregating sites in genetical models without recombination. Theor
983 Popul Biol **7**: 256–276.

984 White M. A., Ané C., Dewey C. N., Larget B. R., Payseur B. A., 2009 Fine-scale phylogenetic discordance
985 across the house mouse genome. PLoS Genet **5**: e1000729.

986 Yang H., Bell T. A., Churchill G. A., Villena F. P.-M. de, 2007 On the subspecific origin of the laboratory
987 mouse. Nat Genet **39**: 1100–1107.

988 Yang H., Wang J. R., Didion J. P., Buus R. J., Bell T. A., Welsh C. E., Bonhomme F., Yu A. H.-T., Nachman
989 M. W., Pialek J., Tucker P., Boursot P., McMillan L., Churchill G. A., Villena F. P.-M. de, 2011 Subspecific
990 origin and haplotype diversity in the laboratory mouse. Nat Genet **43**: 648–655.

991 Yeh T.-C., Liu H.-L., Chung C.-S., Wu N.-Y., Liu Y.-C., Cheng S.-C., 2010 Splicing factor Cwc22 is required
992 for the function of Prp2 and for the spliceosome to escape from a futile pathway. Mol Cell Biol **31**: 43–53.

993

994 # FIGURE LEGENDS

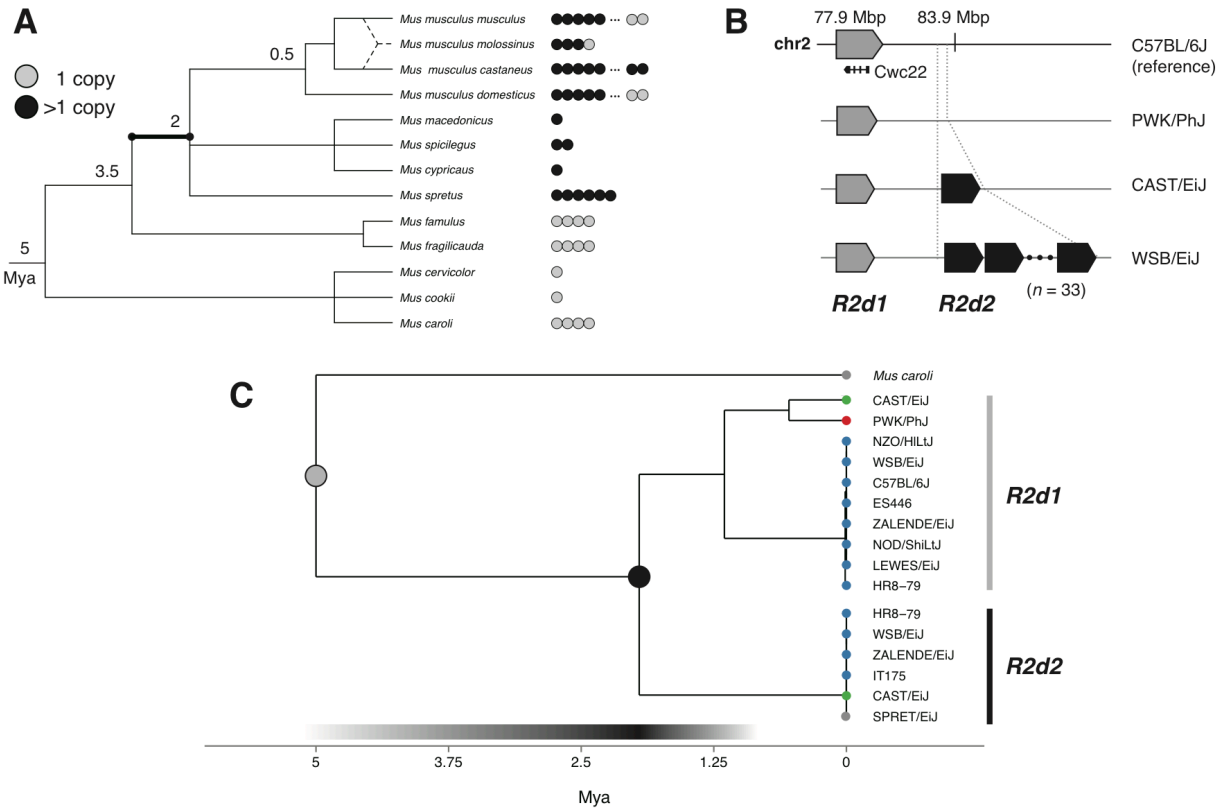

995

996 **Figure 1. Origin and age of the *R2d2* duplication.** (**A**) *R2d* copy number across the phylogeny of the
997 genus *Mus*. Each dot represents one individual; grey dots indicate copy number 1 and black dots copy
998 number >1. The duplication event giving rise to *R2d1* and *R2d2* most likely occurred on the highlighted
999 branch. Approximate divergence times (REF: Suzuki 2004) are given in millions of years ago (Mya) at
1000 internal nodes. (**B**) Schematic structure of the *R2d1-R2d2* locus. The mouse reference genome (strain
1001 C57BL/6J, *M. m. domesticus*) contains a single copy of *R2d* at *R2d1*. Wild-derived inbred strains vary in
1002 copy number from 1 (PWK/PhJ, *M. m. musculus*) to 2 (CAST/EiJ, *M. m. castaneus*) to 33 (WSB/EiJ, *M. m.*
1003 *domesticus*). *R2d1* is located at approximately 77.9 Mbp and *R2d2* at 83.8 Mbp. (**C**) Representative tree
1004 constructed from *de novo* assembled *R2d1* and *R2d2* sequences assuming a strict molecular clock.
1005 Sequences are colored according to their subspecies of origin: *M. m. domesticus*, blue; *M. m. musculus*, red;
1006 *M. m. castaneus*, green; and the outgroup species *M. spretus* in grey. The duplication node is indicated
1007 with a black dot. The 95% HPDI for the age of the duplication event obtained by Bayesian phylogenetic
1008 analysis with BEAST is displayed below the tree.

1009

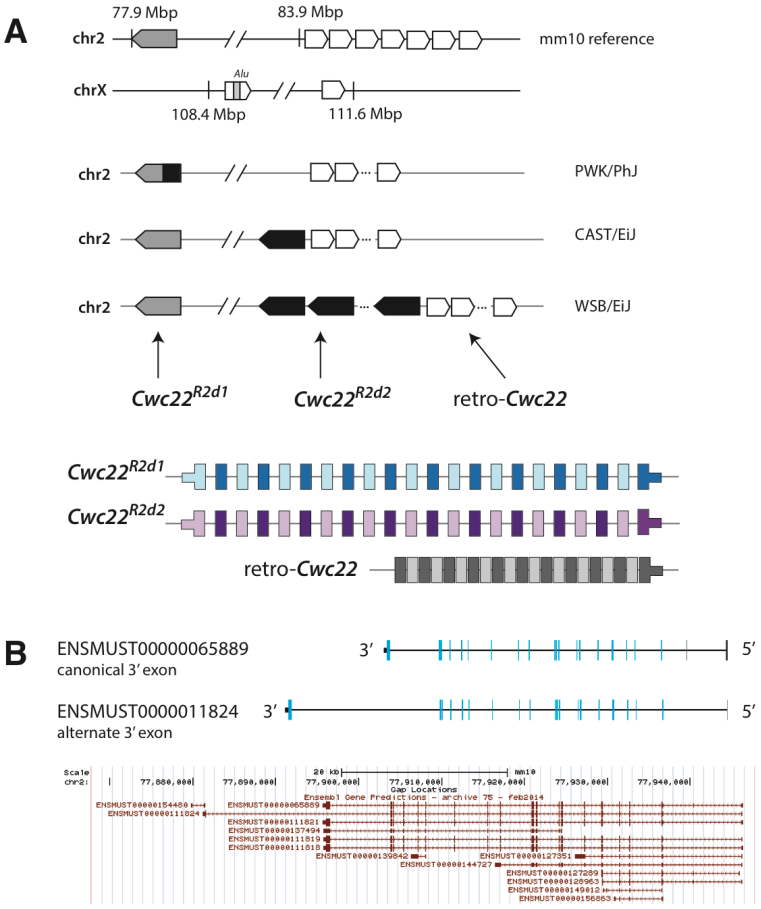

Figure 2. *Cwc22* paralogs in the mouse genome. (**A**) Location and organization of *Cwc22* gene copies present in mouse genomes. The intact coding sequence of *Cwc22* exists in in both *R2d1* (grey shapes) and *R2d2* (black shapes). Retrotransposed copies (empty shapes) exist in two loci on chrX and one locus on chr2, immediately adjacent *R2d2*. Among the retrotransposed copies, coding sequence is intact only in the copy on chr2. (**B**) Alternate transcript forms of *Cwc22*, using different 3′ exons. Coding exons shown in blue and untranslated regions in black. All Ensembl annotated transcripts are shown in the lower panel (from UCSC Genome Browser.)

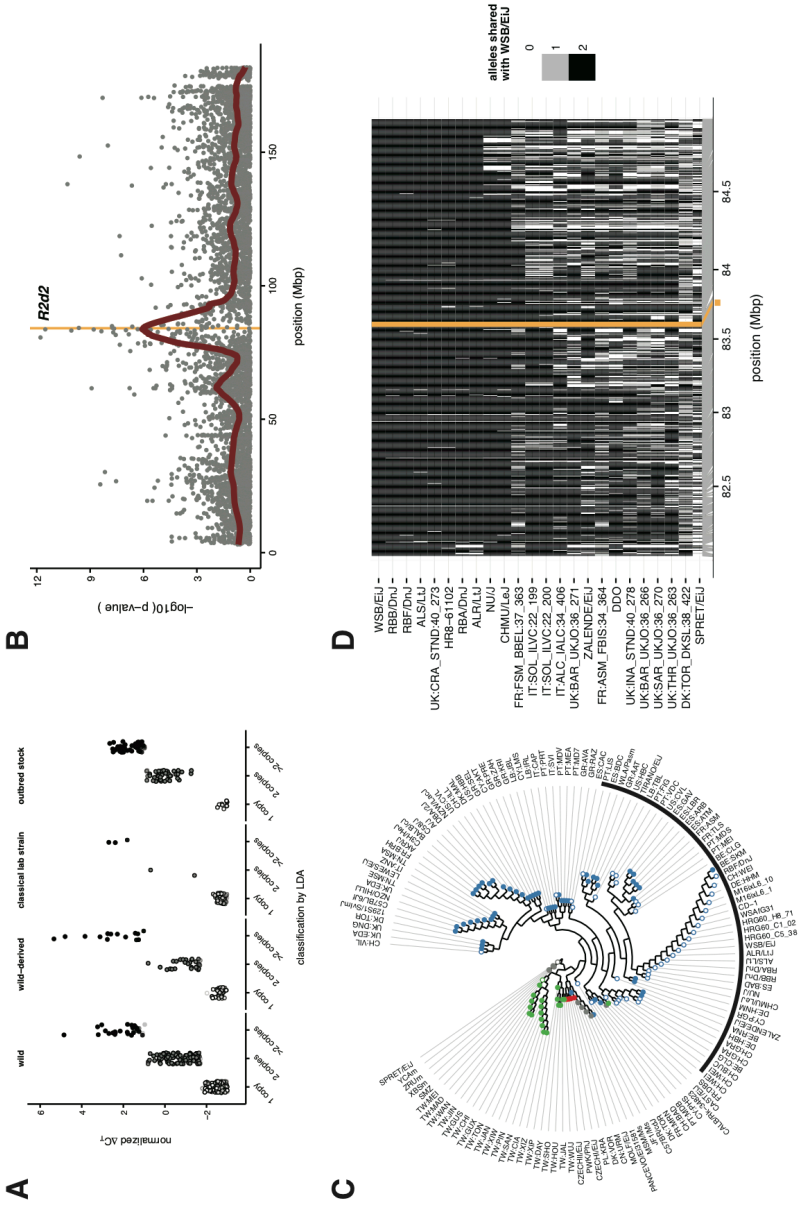

Figure 3. Copy-number variation of *R2d* in mouse populations worldwide. (**A**) Copy-number variation as measured by quantitative PCR. The normalized deltaCt value is proportional to log2(copy number). Samples are classified as having 1 copy, 2 copies or >2 copies of *R2d* using linear discriminant analysis (LDA). (**B**) Fine-mapping the location of *R2d2* in 83 samples genotyped on the Mouse Diversity Array (MDA). Grey points give nominal p-values for association between *R2d* copy number and genotype; red points show a smoothed fit through the underlying points. The candidate interval for *R2d2* from Didion *et al.* (2015), shown as an orange shaded box, coincides with the association peak. (**C**) Local phylogeny at chr2: 82-85 Mbp in 135 wild-caught mice and wild-derived strains. Tips are colored by subspecies of origin: *M. m. domesticus*, blue; *M. m. musculus*, red; *M. m. castaneus*, green; other taxa, grey. Individuals with >2 copies of *R2d* are shown as open circles. Black arc indicates the portion of the tree enriched for individuals with high copy number. (**D**) Haplotypes of laboratory strains and wild mice sharing a high-copy allele at *R2d2*. All samples share a haplotype over the region shaded in orange.

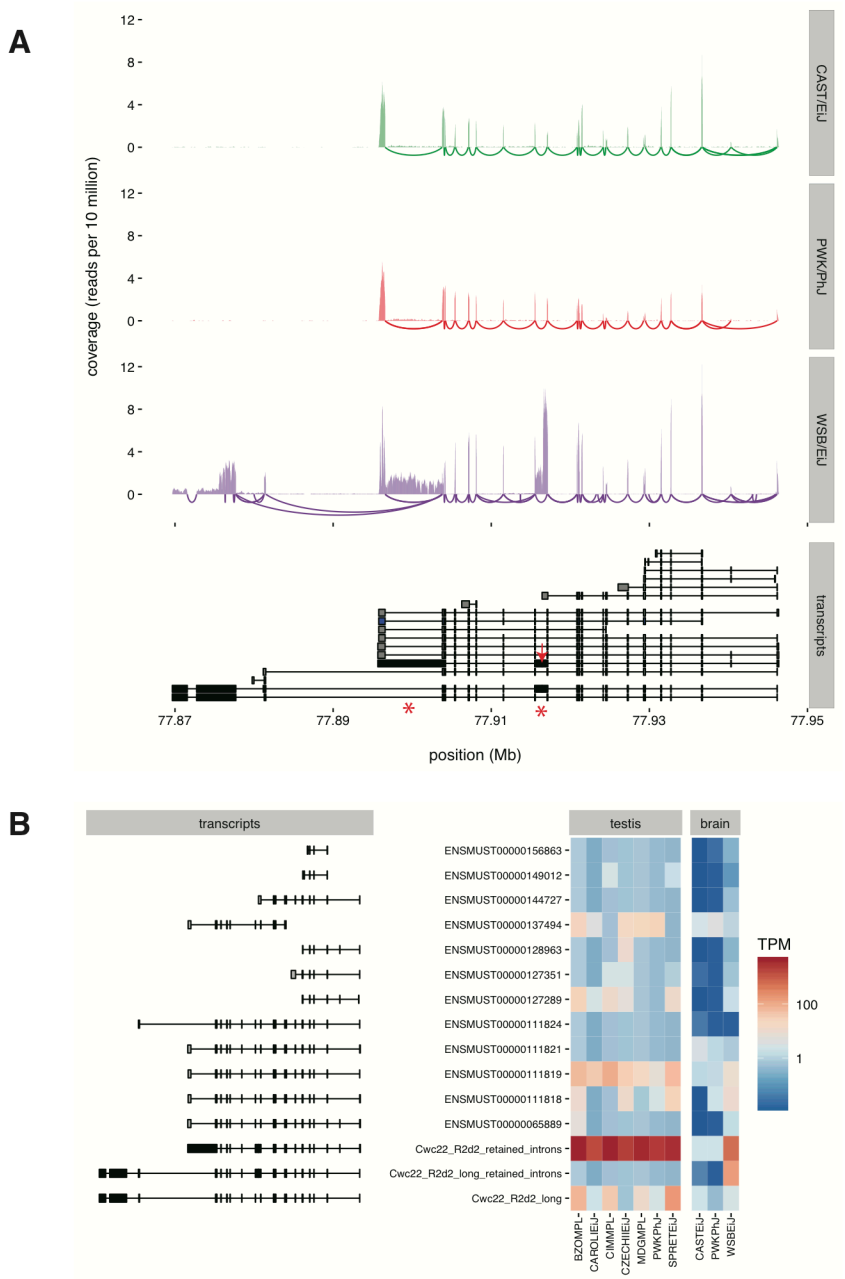

Figure 4. Expression of *Cwc22* isoforms. (**A**) Read coverage and splicing patterns in *Cwc22* in adult mouse brain from three wild-derived inbred strains. Swoops below x-axis indicate splicing events supported by 5 or more split-read alignments. Known transcripts of $Cwc22^{R2d1}$ (grey, from Ensembl), inferred transcripts from $Cwc22^{R2d2}$ (black) and the sequence of retro-*Cwc22* mapped back to the parent gene (blue) are shown in the lower panel. Red stars indicate retained introns; red arrow indicates insertion site of an ERV in *R2d2*. (**B**) Estimated relative expression of *Cwc22* isoforms (y-axis) in adult mouse brain and testis in wild-derived inbred strains (x-axis). TPM, transcripts per million, on log10 scale.

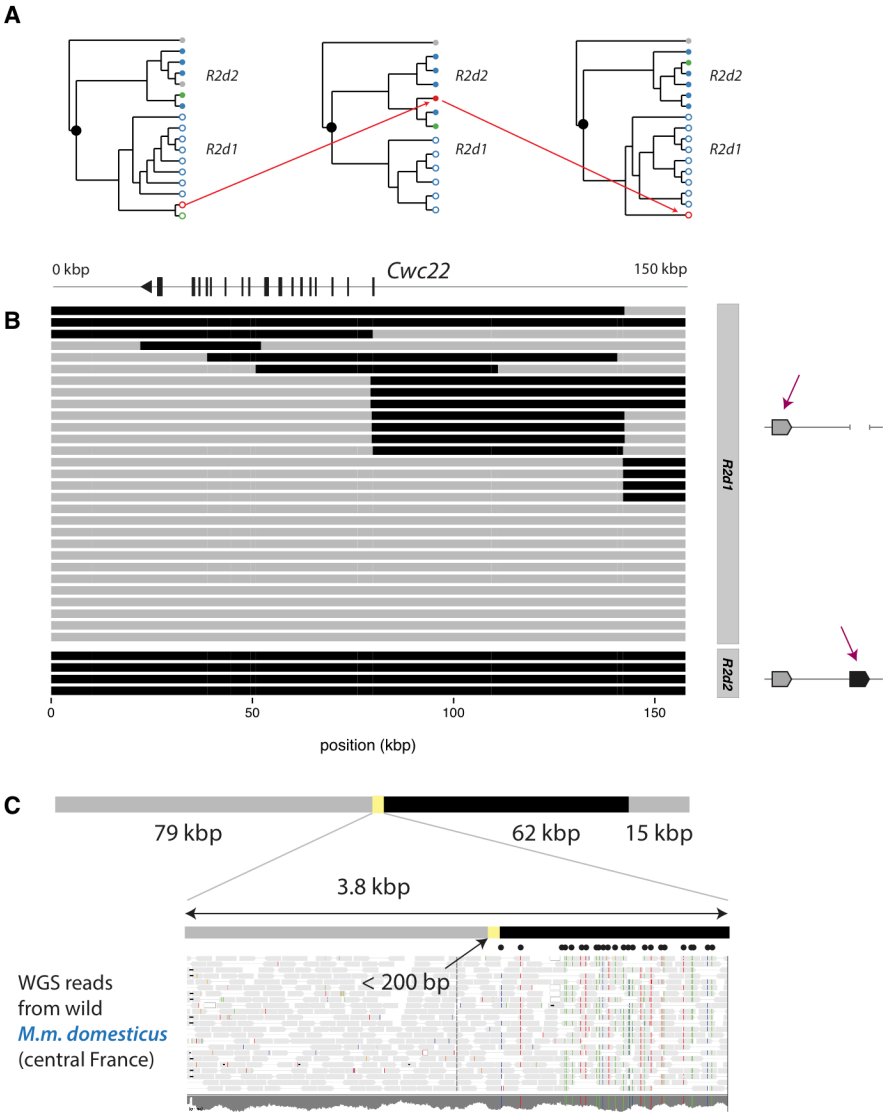

Figure 5. Signatures of non-allelic gene conversion between *R2d1* and *R2d2*. (**A**) Phylogenetic trees for three representative intervals across *R2d*. Sequences are labeled according to their subspecies of origin using the same color scheme as in **Figure 1**; open circles are *R2d1*-like sequences and closed circles are *R2d2*-like**.** Trees are drawn so that *M. caroli*, the outgroup species used to root the trees, is always positioned at the top. The changing affinities of PWK/PhJ (red) and CAST/EiJ (green) along *R2d* are evidence of non-allelic gene conversion. (**B**) *R2d* sequences from 20 wild-caught mice and 5 laboratory inbred strains. Each track represents a single chromosome; grey regions are classified as *R2d1*-like based on manual inspection of sequence variants, and black-regions *R2d2*-like. Upper panel shows sequences from samples with a single copy of *R2d*, residing in *R2d1*. Lower panel shows representative *R2d2* sequences for comparison. (**C**) Read alignments at the boundary of a non-allelic gene conversion tract. The *R2d1* sequence from a single chromosome from mouse trapped in central France is a mosaic of *R2d1*-like (grey) and *R2d2*-like (black) segments. A magnified view of read pairs in the 3.8 kbp surrounding the proximal boundary of the tract (generated with IGV) reveals read pairs spanning the junction. Black dots indicate the position of derived alleles diagnostic for *R2d2*. The precise breakpoint lies somewhere in the yellow shaded region between the last *R2d1*-specific variant and the first *R2d2*-specific variant.

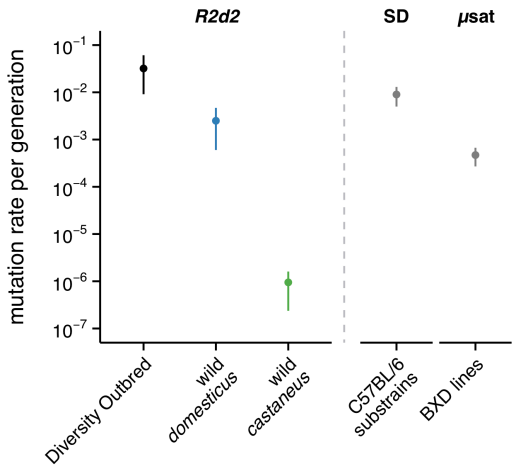

1058

1059 **Figure 6. Rate of *de novo* copy-number changes at *R2d2*.** Estimates of per-generation mutation rate for
1060 CNVs at *R2d2* (±1 bootstrap SE) in the Diversity Outbred population; among wild *M. m. domesticus;* and
1061 among wild *M. m. castaneus*. For comparison, mutation rates are shown for the CNV with the highest rate
1062 of recurrence in a C57BL/6J pedigree (Egan *et al.* 2007) and for a microsatellite whose mutation rate was
1063 estimated in the BXD panel (Dallas 1992).

1064

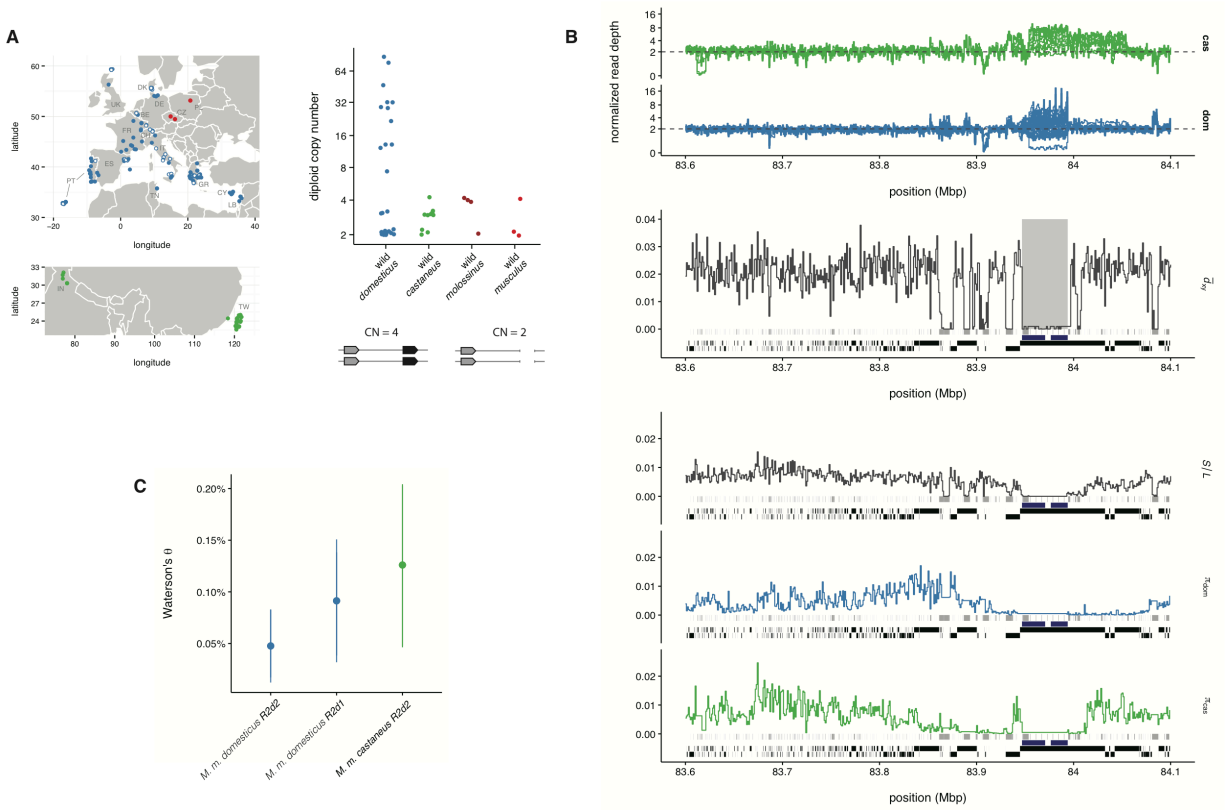

Figure 7. Sequence and structural diversity around *R2d2*. (**A**) Geographic origin of wild mice used in this study, color-coded by subspecies (blue, *M. m. domesticus*; red, *M. m. musculus*; green, *M. m. castaneus*). Diploid copy number of the *R2d* unit is shown for wild samples for which integer copy-number estimates are available: 26 *M. m. domesticus* and 10 *M. m. castaneus* with whole-genome sequencing data, and representatives from *M. m. molossinus* and *M. m. musculus* for comparison. Schematic shows the *R2d1*/*R2d2* configurations corresponding to diploid copy numbers of 2 and 4. (**B**) Profiles of read depth (first panel), average sequence divergence to outgroup species *M. caroli* (d_{xy}, second panel), number of segregating sites per base (S/L, third panel) and within-population average heterozygosity (π, fourth panel). The region shown is 500 kbp in size and centered on the insertion site of *R2d2*. Grey boxes along baseline show positions of repetitive elements (from UCSC RepeatMasker track); black boxes show non-recombining haplotype blocks. Blue bars indicate the position of 7 tandem duplications in the mm10 reference sequence with >99% mutual identity, each containing a copy of retro-*Cwc22*. The duplications are absent in *M. caroli* (indicated by grey shaded box.)

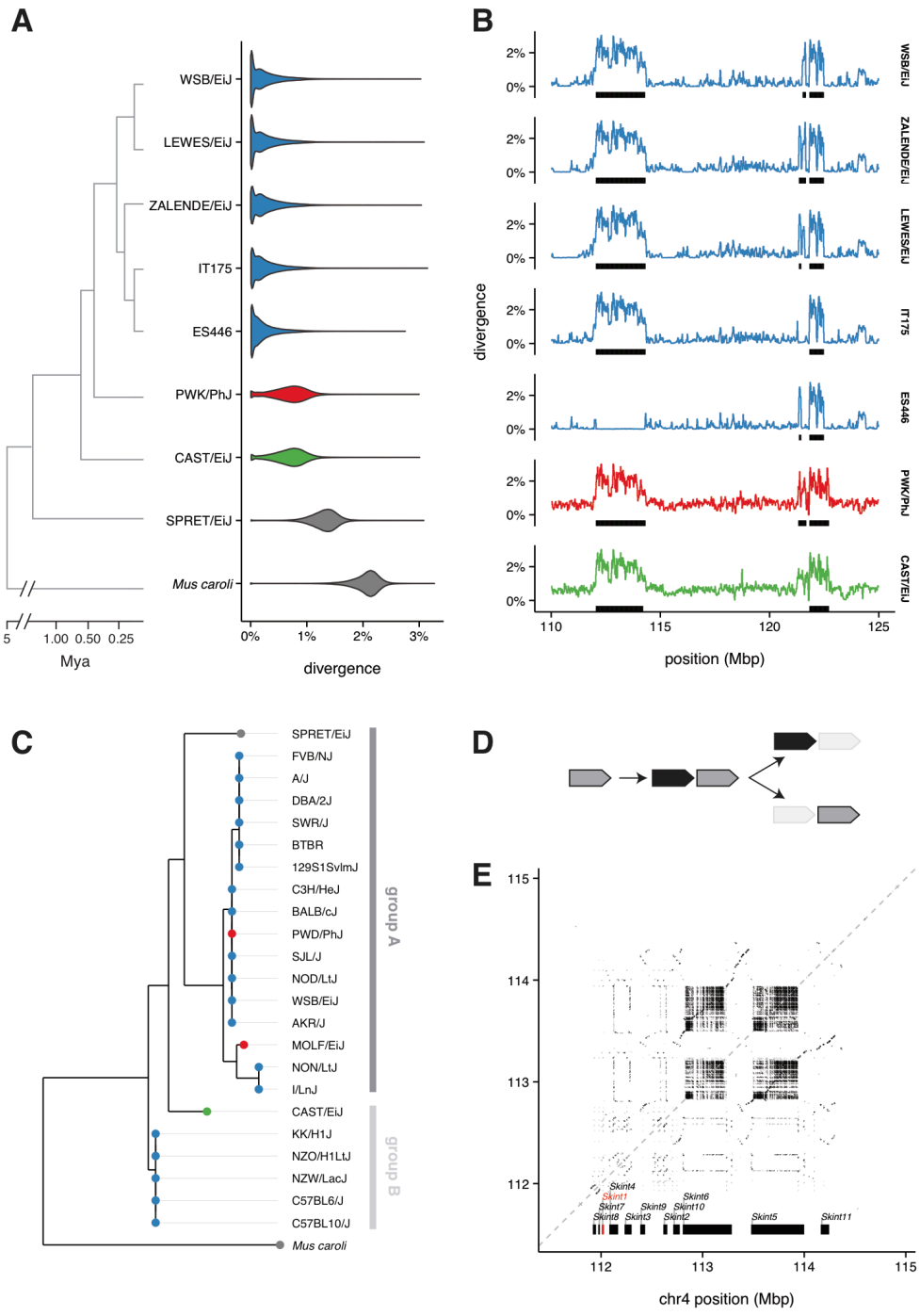

Figure 8. (**A**) Genome-wide sequence divergence estimates for representative samples from the sub-genus *Mus*. (**B**) Estimated sequence divergence in 31 kbp windows across distal chr4 for the samples in panel A. Divergent regions identified by the hidden Markov model (HMM) are indicated with black bars along the horizontal axis. (**C**) Phylogenetic tree constructed from *Skint1* coding sequences reported in Boyden *et al.* (2008) (**D**) Schematic representation of the process of gene duplication, followed by differential loss of paralogs along independent lineages. (**E**) Dotplot of self-alignment of sequence from the region of distal chr4 containing the *Skint* gene family. Positions of *Skint* genes are indicated along the horizontal axis; *Skint1* highlighted in red.

SUPPLEMENTARY MATERIAL

Supplementary Figure 1. Conservation of synteny between mouse and four other mammals around *Cwc22*^{R2d1} (upper panel) indicates that the *R2d1* sequence remains in its ancestral position. Chevrons represent genes, alternating white and grey, and are oriented according to the strand on which the gene is encoded. *Cwc22*^{R2d2} is novel in the mouse but its position relative to genes with conserved order is shown in the lower panel. Note that synteny is disrupted in mouse and rat distal to *R2d2*.

Supplementary Figure 2. Pairwise alignment of *R2d2* contig (top) to the *R2d1* reference sequence (bottom). Dark boxes show position of repetitive elements present in both sequences; syntenic positions are connected by grey anchors, and blank space represents aligned bases in both sequences. Orange boxes indicate position of repetitive elements present in the *R2d1* sequence but not detected in *R2d2*; blue boxes indicate position of elements in *R2d2* but not *R2d1*. *Cwc22* transcripts are shown below the alignment.

Supplementary Figure 3. Phylogenetic tree constructed from amino acid sequences for mammalian *Cwc22* homologs (including all three mouse paralogs) with chicken as an outgroup. Node labels indicate support in 100 bootstrap replicates.

Supplementary Figure 4. Alignment of amino acid sequences from mouse *Cwc22*^{R2d1}, *Cwc22*^{R2d2} and retro-*Cwc22*, plus *Cwc22* orthologs from 19 other placental mammals plus opossum, platypus and chicken as outgroups. Residues are colored according to biochemical properties and gaps are shown in grey. Information content of each column in the alignment, measured as the Jenson-Shannon divergence, is plotted in the lower panel.

Supplementary Figure 5. Gene conversion tracts identified by *de novo* assembly. (**A**) Phylogenetic trees for twelve intervals across *R2d*. Samples are labeled according to their subspecies of origin using the same color scheme as in **Figure 1.** Trees are drawn so that *M. caroli*, the outgroup species used to root the trees, is always positioned at the top. The changing affinities of PWK/PhJ (red) and CAST/EiJ (green) along *R2d* is evidence of non-allelic gene conversion. (**B**) Inspection of derived alleles diagnostic for *R2d1* or *R2d2* reveals conversion tracts. Each horizontal track represents a haplotype, and each dot a variant site. Filled dots are fully diagnostic for *R2d1* or *R2d2*; open circles are partially-informative. Positions with *R2d1*-like sequence are colored grey, and those with *R2d2*-like sequence colored black. Conversion tracts are indicated by yellow boxes. Physical positions of variant sites within *R2d* are shown with respect to the *R2d1* sequence present in the mouse reference genome. The *Cwc22* gene spans conversion tracts in multiple samples.

Supplementary Figure 6. Partial loss of *R2d2* with structural rearrangement. (**A**) Inferred structure of the *R2d1-R2d2* region in IR:AHZ_STND:015, a wild *M. m. domesticus* individual from Iran. *R2d1* is present on both chromosomes but only a fragment of *R2d2* remains on one chromosome, and it has been transposed into the retro-*Cwc22* array. (**B**) Normalized depth of coverage (2 = normal diploid level) across *R2d*. Regions in grey represent reads from *R2d1* alone, while region in black captures reads from *R2d1* and *R2d2*, as shown by arrows from panel A. (**C**) Position of read pairs (red; not drawn to scale) with soft-clipped alignments to *R2d1*. The proximal read aligns in the 3′ UTR of *Cwc22*, and the distal read across an exon-intron boundary within the gene body. Note the "outward"-facing direction of the alignments. (**D**) Positions of the mates of the reads in panel C. Note that the x-axis is reversed so that the exons of retro-*Cwc22* (encoded on the plus strand) parallel those of *Cwc22* (encoded on the minus strand). The 3′ read maps across the boundary of th 3′ UTR of *Cwc22* and the ERV mediating the retrotransposition event. The 5′ read maps across two exon-exon boundaries in retro-*Cwc22*, so there is no ambiguity regarding its alignment to the retro-transposed copy. (**E**) Inferred structure of *Cwc22* paralogs in this

sample. Note that one of the copies of retro-*Cwc22* is now a mosaic of retrotransposed and $Cwc22^{R2d2}$-derived sequence.

Supplementary Figure 7. Suppression of crossing-over around *R2d2*. (**A**) Difference between expected and observed recombination fraction between markers flanking *R2d2* in experimental crosses in which at least one parent is segregating for a high-copy allele of *R2d2*. Thick and thin vertical bars show 90% and 95% confidence bounds, respectively, obtained by non-parametric bootstrap. (**B**) Cumulative recombination map in the middle region of chr2 obtained from 4,640 Diversity Outbred mice. Recombination events involving the WSB/EiJ haplotype (*R2d2* copy number 33) are shown in purple and all other events in grey. Maps are normalized such that they begin and end at the same value.

Supplementary Figure 8. Targeted *de novo* assembly using the multi-string Burrows-Wheeler Transform (msBWT). (**A**) The msBWT and its associated FM-index implicitly represent a suffix array of sequencing reads, such that read suffixes sharing a k-mer prefix are adjacent in the data structure. This allows rapid construction of a local de Bruijn graph starting from a k-mer seed (dark blue) and extending by successive k-mers (light blue) containing the $(k-1)$-length suffix of the previous k-mer. A $(k-1)$-length prefix with more than one possible suffix (red and orange) creates a branch point. Adjacent nodes in the graph with in-degree and out-degree one can be collapsed into a single node, yielding a simplified graph, which can then be traversed to obtain linear contig(s). (**B**) Paralogs of *R2d* can be disentangled using the local de Bruijn graph by exploiting differences in copy number. Edges in the graph are weighted by read count, and linear contigs for the *R2d1* and *R2d2* paralogs obtained by traversing the graph in a manner that minimizes the variance in edge weights along possible paths. Phase-informative reads (those overlapping multiple paralogous variants) provide a second source of evidence.

Supplementary Table 1. List of mouse samples used in this study, with their taxonomic designation, geographic origin and *R2d2* copy-number classification.

Supplementary Table 2. Transposable-element insertions private to *R2d1* or *R2d2*. Coordinates are offsets with respect to the start position of *R2d* (for *R2d1*: chr2: 77,869,657 in the reference genome; for *R2d2*: the beginning of the *de novo* assembled contig in **Supplementary File 1**.)

Supplementary Table 3. Individuals from the Diversity Outbred population carrying *de novo* copy-number mutations at *R2d2*. Each was expected to be heterozygous for the WSB/EiJ allele (33 haploid copies).

Supplementary Table 4. Regions of excess divergence between wild or wild-derived mice and the mouse reference genome (GRCm38/mm10 build).

Supplementary Table 5. Regions of R2d targeted for *de novo* assembly in inbred strains.

Supplementary File 1. Compressed archive containining *R2d2* contig (from WSB/EiJ) and multiple sequence alignments from selected regions in **Supplementary Table 5**.